Towards consistent seismological models of the core-mantle boundary landscape

P. Koelemeijer[a,b,*]

[a] *Department of Earth Sciences, Royal Holloway University of London, Egham, UK*
[b] *Department of Earth Sciences, University College London, London, UK*

Keywords: Core-mantle boundary, Topography, Density structure, Seismic tomography, Normal modes

[*] Corresponding author: P. Koelemeijer, paula.koelemeijer@rhul.ac.uk

In press in Marquardt et al. (eds): "Mantle Convection and Surface Expressions", AGU Monograph, 2020

Abstract

The dynamic topography of the core-mantle boundary (CMB) provides important constraints on dynamic processes in the mantle and core. However, inferences on CMB topography are complicated by the uneven coverage of data with sensitivity to different length scales and strong heterogeneity in the lower mantle. Particularly, a trade-off exists with density variations, which ultimately drive mantle flow and are vital for determining the origin of mantle structures. Here, I review existing models of CMB topography and lower mantle density, focusing on seismological constraints. I develop average models and vote maps with the aim to find model consistencies and discuss what these may teach us about lower mantle structure and dynamics. While most density models image two areas of dense anomalies beneath Africa and the Pacific, their exact location and relationship to seismic velocity structure differs between studies. CMB topography strongly influences the retrieved density structure, which helps to resolve differences between recent studies based on Stoneley modes and tidal measurements. Current CMB topography models vary both in pattern and amplitude and a discrepancy exists between models based on body-wave and normal-mode data. As existing models feature elevated topography below the Large-Low-Velocity Provinces (LLVPs), very dense compositional anomalies may currently be ruled out as possibility. To achieve a similar consistency as observed in lower mantle models of S-wave and P-wave velocity, future studies should combine multiple data sets to break existing trade-offs between CMB topography and density. Important considerations in these studies should be the choice of theoretical approximation and parameterisation. Efforts to develop models of CMB topography consistent with body-wave, normal-mode and geodetic data should be intensified, which will aid in narrowing down possible explanations for the LLVPs and provide additional insights into mantle dynamics.

1. Introduction

The Earth's surface exhibits a range of features that reflect the fact that we live on a dynamic planet. Dynamic surface topography informs us about mantle flow and upwellings (Austermann & Hoggard, this volume). Similarly, the landscape of the core-mantle boundary (CMB), the largest physical and chemical boundary within the Earth located ∼3000 km below

our feet, holds important clues for understanding the nature and evolution of mantle flow.

Lateral variations in CMB topography break the symmetry of the dynamic regime in the outer core and are linked to lateral heat flow variations, thereby influencing core flow and possibly the geodynamo (e.g. Gubbins and Richards, 1986; Calkins et al., 2012; Davies et al., 2014; Tarduno et al., 2015). The pressure torque induced by topography has been thought to give rise to length-of-day variations (e.g. Jault and Le Mouël, 1990; Hide et al., 1993; Kuang and Bloxham, 1993; Asari et al., 2006; Dehant et al., 2017) by transferring angular momentum between the mantle and core (see Buffett, 2015, for a review of possible core-mantle interactions). In addition, estimates of CMB topography aid in constraining mantle viscosity (e.g. Yoshida, 2008; Steinberger and Holme, 2008). Furthermore, Deschamps et al. (2018) suggested that accurate constraints on CMB topography could provide complimentary insights into the density structure of the lower mantle.

Studies of CMB topography have been performed since the 1970s, constraining topographic variations on 10-1000 km length scales, as discussed more in Section 2. Important constraints are provided by the traveltimes of seismic body waves that reflect or refract along the boundary (e.g. Menke, 1986; Garcia and Souriau, 2000; Koper et al., 2003; Rost and Revenaugh, 2004; Tanaka, 2010; Colombi et al., 2014; Soldati et al., 2012), while observations of seismic energy scattered by small-scale variations provide additional insights on the roughness of the boundary (e.g. Haddon and Cleary, 1974; Doornbos, 1978; Bataille et al., 1990; Earle and Shearer, 1998; Shearer et al., 1998; Mancinelli and Shearer, 2016). Constraints on longer wavelengths come from observations of normal modes (Earth's free oscillations) as well as from geodetic data (e.g. Hide and Horai, 1968; Hager et al., 1985; Gwinn et al., 1986; Li et al., 1991; Jault and Le Mouël, 1990; Forte et al., 1995; Ishii and Tromp, 1999; Mathews et al., 2002; Koelemeijer et al., 2017). Numerical modelling of mantle flow and the induced dynamic topography aids in the interpretation of these observational constraints (e.g. Forte, 2007; Yoshida, 2008; Steinberger and Holme, 2008; Simmons et al., 2009; Lassak et al., 2010; Liu and Zhong, 2015; Deschamps et al., 2018).

Despite a range of sensitive data and a plethora of models, existing models of CMB topography continue to differ in both pattern and amplitude (see also Section 2). This is primarily because the data employed in studies of CMB topography are also sensitive to lower mantle structures, requiring joint inversions or corrections. However, the lower mantle is highly heterogeneous, mimicking the complexities found in the upper boundary layer of the mantle, as discussed in various other chapters in this volume. Many ex-

cellent reviews cover the range of seismological structures that have been imaged on different spatial scales in the lower mantle, including observations of seismic reflectors, anisotropy, scattering and ultra-low-velocity zones (Forte, 2007; Garnero and McNamara, 2008; Hernlund and McNamara, 2015, e.g.), which are therefore not repeated here. However, it is worth briefly noting the most pronounced features on the longest wavelengths and the debate that surrounds them.

Two antipodal regions of lower-than-average seismic velocity are imaged underneath the Pacific and Africa (Figure 1), covering about 25 % of the core surface and rising up to ∼1000 km above the core (Garnero and McNamara, 2008; Cottaar and Lekic, 2016; Garnero et al., 2016). Initially dubbed LLSVPs for large-low-*shear*-velocity-provinces (LLSVPs) due to their low S-wave velocities (V_S), these structures should now be referred to as LLVPs (large-low-velocity-provinces, adopted here as well), as they are also observed to have low P-wave velocities (V_P) (e.g. Koelemeijer et al., 2016; Garnero et al., 2016). The LLVPs are imaged consistently in different tomographic models (Figure 1), as demonstrated using cross-model correlation (Becker and Boschi, 2002), clustering analysis (Lekić et al., 2012; Cottaar and Lekic, 2016) and vote maps (Shephard et al., 2017). However, several questions regarding their origin, longevity and influence on mantle dynamics are still debated: Can their seismic properties be solely explained by thermal variations or are large-scale chemical variations required? If they are chemically distinct, what is their intrinsic density and how do density variations vary within these structures? Have they been present since the formation of the Earth or have they formed from the accumulation of subducted oceanic crust or reaction products between the core and mantle? Are they large-scale coherent structures or are they made up of several smaller structures? The answers to these questions are important as the LLVPs have a large influence on global mantle dynamics (e.g. Dziewonski et al., 2010; Davies et al., 2012; Bower et al., 2013; Nakagawa and Tackley, 2014), changing the cooling efficiency of the mantle (Nakagawa and Tackley, 2014), altering the heat flow distribution at the CMB and thus potentially inducing magnetic field reversals (e.g. Zhang and Zhong, 2011; Olson et al., 2015).

To unravel the nature of the LLVPs, knowledge of more than one elastic parameter is needed, i.e. constraints on V_P, bulk-sound velocity V_C or density ρ are required in addition to V_S. Observations of a high ratio of V_S over V_P variations and its distribution at a given depth, as well as a negative correlation between V_S and V_C variations in the lower mantle have often been interpreted as evidence for chemically distinct LLVPs (e.g. Karato and Karki, 2001; Su and Dziewonski, 1997; Ishii and Tromp, 1999; Masters et al.,

2000a; Deschamps and Trampert, 2003; McNamara and Zhong, 2005; Houser et al., 2008). However, more recent studies have indicated that the V_S/V_P ratio or its distribution do not provide constraints on mantle composition and that a lower mantle phase transition can also explain the negative correlation between V_S and V_C variations (Tesoniero et al., 2016; Koelemeijer et al., 2018). Many arguments exist for either side of the debate, with evidence from geochemical data for the presence of an unmixed primordial reservoir in the mantle (e.g. Zindler and Hart, 1986; Hofmann, 1997; Mukhopadhyay, 2012; Rizo et al., 2019), geodynamical simulations supporting either possibility (e.g. Forte and Mitrovica, 2001; Schubert et al., 2004; Schuberth et al., 2009; Davies et al., 2012; McNamara and Zhong, 2004, 2005; McNamara et al., 2010; Deschamps et al., 2011; Nakagawa et al., 2012; Li et al., 2014; Nakagawa and Tackley, 2014; Davies et al., 2015b) and the geographical correlation between LLVPs and surface features related to mantle upwellings being interpreted in different ways (e.g. Burke et al., 2008; Torsvik et al., 2010; Austermann et al., 2014; Davies et al., 2015a). This ongoing debate has been perfectly well summarised by many recent reviews (e.g. Davies et al., 2015b; Hernlund and McNamara, 2015; Garnero et al., 2016), and will therefore not be repeated in detail here.

Robust constraints on LLVP density structure have been at the centre of the debate regarding the origin of the LLVPs (e.g. Davies et al., 2015b; Garnero et al., 2016; Lau et al., 2017; Koelemeijer et al., 2017), as an increased density in combination with low seismic velocities would unequivocally point to a thermochemical nature (Karato and Karki, 2001). Knowledge of lower mantle density is also important to understand the driving forces of mantle flow and for studies of CMB topography, which are inherently linked to each other through isostasy and dynamic flow, often giving rise to a strong trade-off in observational data sets.

While density variations are vital for understanding lower mantle dynamics, they are not easy to determine from seismological data. Body wave data are only indirectly sensitive to density, while surface waves only provide constraints on upper mantle structure. Density models are therefore primarily constructed from normal-mode or geodetic observations, with several lower mantle models existing in the literature (e.g. Ishii and Tromp, 1999; Trampert et al., 2004; Mosca et al., 2012; Moulik and Ekström, 2016; Koelemeijer et al., 2017; Lau et al., 2017). However, there remains controversy regarding the density of the LLVPs, whether they are lighter or denser than the ambient mantle and what the depth-extent of a dense layer is, as discussed further in Section 3.

The aim of this contribution is to review the large-scale seismological

landscape of the core-mantle boundary. Lower mantle V_S and V_P variations are now consistently imaged on large-scales (Lekić et al., 2012; Cottaar and Lekic, 2016), as demonstrated in Figure 1 for tomographic models developed since 2010. This chapter focuses on some remaining questions: how much progress have been made on CMB topography and density? How consistent are our images after 35 years of CMB topography studies and 20 years since the first model of lateral density variations in the mantle? First of all, I will review studies of CMB topography and density, focusing on seismological results, as recent reviews (Hernlund and McNamara, 2015; Deschamps et al., 2018) and other chapters in this volume already focus on dynamical aspects of lowermost mantle structure. Subsequently, I will analyse existing topography and density models in a quantitative way, identify consistent features and discuss the insights these provide about deep mantle structure and dynamics. Finally, I will discuss future directions for reconciling differences and developing consistent models of the core-mantle boundary landscape.

2. Existing models of CMB topography

This overview primarily follows historical developments (see also Table 1), e.g. starting with early studies of CMB topography based on scattered waves, core-reflected (PcP, ScS), core-refracted (PKP, PKKP, PKmP) and inner core (PKIKP, PKiKP) phases. This is followed by a discussion of global CMB topography models developed using body-wave and normal-mode data. As I focus on seismological insights, I only briefly discuss geodynamic predictions and other insights towards the end of this section.

2.1. Regional CMB topography studies

The first studies of CMB topography arose in the 1970s from the detailed analysis of precursors of core-refracted phases recorded (see Bataille et al., 1990; Loper and Lay, 1995, for a review of these early studies). The classic studies of Haddon (1972) and Cleary and Haddon (1972) first recognised that the onset of PKP precursors required scattering from small-scale heterogeneities near the CMB, confirmed by the analysis of PKP and PKKP precursors in subsequent studies (Doornbos and Vlaar, 1973; Doornbos, 1974). Haddon and Cleary (1974) first raised the possibility that ∼200 m bumps on the core with 10–20 km length scales could explain the data. Follow-up studies investigating PKP and PKKP precursors found similar topography values (e.g. Doornbos, 1976, 1978; Van den Berg et al., 1978; Doornbos, 1980; Bataille and Flatté, 1988), although results based on PmKP (Aleshin and Vinnik, 1975) and PKKP backscattered precursors (Chang and Cleary,

1978, 1981) hinted at larger topography values of a few km. Since the 1990s, there has been a constant interest in PKP and PKKP precursors, with studies moving towards more global analysis and shorter wavelengths (e.g. Bataille et al., 1990; Earle and Shearer, 1998; Shearer et al., 1998; Mancinelli and Shearer, 2016).

Scattering studies provide excellent constraints on small-scale roughness of the CMB (wavelengths of 7–30 km), but the analysis of other seismic phases is required to determine topographic variations on longer wavelengths. Menke (1986) was the first to utilise core-reflected phases (PcP amplitude dependence) in the study of CMB topography, finding undulations of a few 100 m on short length scales (10 km). Core-reflected phases were studied further, often by considering PcP/P amplitude ratios or their simple pulse shapes, to find topographic variations of up to 3 km on wavelengths of 50–400 km (Neuberg and Wahr, 1991; Vidale and Benz, 1992; Emmerich, 1993; Rost and Revenaugh, 2004). Recent regional studies on PcP and ScP arrivals have suggested a range of amplitudes; Wu et al. (2014) found a best fit for a depression of 6 km over 300–400 km under Alaska, while Shen et al. (2016) concluded that topography of 1.2 km on length scales of 140 km was required to fit their seismic observations under Japan. These studies indicate that topography values found in individual studies vary significantly and depend strongly on length scale and location.

With an increase in the number of body-wave observations, issues with their interpretations in terms of CMB topography were identified. Particularly, it proved difficult to separate out the topography effect from lower mantle structure (Kampfmann and Müller, 1989; Murphy et al., 1997). Furthermore, a bias in traveltime data due to focusing and unfocusing was identified (Rekdal and Doornbos, 1992; Emmerich, 1993). To overcome some of these issues, joint studies of PcP observations and core-refracted phases were performed (e.g. Gudmundsson, 1989; Rekdal and Doornbos, 1992). Specifically, the study of Garcia and Souriau (2000) combined PcP, PKP and PKKP observations to deduce that 95 % of the core surface was between -4.0 and 4.0 km on wavelengths of 300 to 1500 km. Differential traveltime measurements relative to direct arrivals (e.g. PcP–P) or inner core phases (e.g. PKP–PKIKP, PKiKP–PcP) were also utilised to minimise the influence of mantle structure (e.g. Neuberg and Wahr, 1991; Poupinet et al., 1993; Koper et al., 2003). Furthermore, with the development of independent tomographic models of lower mantle structure, these were adopted to test the influence of velocity heterogeneity in synthetic examples (Emmerich, 1993; Murphy et al., 1997) or to correct traveltime residuals for mantle structure (Garcia and Souriau, 2000; Koper et al., 2003).

In the last decade, increases in computational power have led to a renewed interest in body-wave studies of CMB topography, accompanied by several advances in theory and methodologies. Using waveform synthetics rather than ray theory, Colombi et al. (2012) and Colombi et al. (2014) studied the sensitivity of different phases to CMB topography and performed waveform inversions, while Ventosa and Romanowicz (2015) illustrated the importance of improved stacking techniques for measuring core-reflected phases. At the same time, improved instrumentation enables observations of phases such as P4KP and P7KP, which, when used in differential traveltime measurements, are less affected by mantle heterogeneity (Tanaka, 2010; Schlaphorst et al., 2015). Although difficult to interpret due to their multiple bounce points, such exotic phases lead to new ideas and methodologies that can be employed in future work.

2.2. Global body-wave models of CMB topography

Body-wave studies of CMB topography based on core-reflected and core-refracted phases, as discussed in the previous section, are naturally done on a regional scale. However, the resulting traveltime measurements that provide information on the depth to the CMB, are often incorporated into global models, which I will now discuss (see also Table 1 and Figure 2a).

The first global models of CMB topography were developed by Creager and Jordan (1986) and Morelli and Dziewonski (1987), both making use of arrival times reported by the Bulletins of the International Seismological Centre (ISC). Morelli and Dziewonski (1987), combining PKP_{bc} data with PcP observations, found topography amplitudes of 6 km (Figure 2a). In contrast, Creager and Jordan (1986) only used core-refracted data (PKP_{ab} and PKP_{df}) and obtained significantly larger amplitudes (peak-to-peak amplitude of 20 km), which they concluded were too large to be due to dynamic topography. These studies typically performed a least-squares inversion after correcting traveltime residuals for mantle heterogeneity using a long-wavelength velocity model. Recognising the influence of lowermost mantle structure, Doornbos and Hilton (1989) additionally inverted for velocity variations in the lowermost mantle, finding that this reduced topography amplitudes.

These early global models were followed by critical studies, that argued that no reliable topography model could be obtained from ISC data (Rodgers and Wahr, 1993; Gudmundsson and Clayton, 1991). This was likely due to discrepancies between different seismic phases (particularly PcP and PKP/PKKP) as a consequent of heterogeneous mantle structure. In addition, Pulliam and Stark (1993) showed that spurious topographic

variations arose from fitting long-wavelength spherical harmonics to patchy body-wave observations, as commonly done in these studies. Furthermore, Stark and Hengartner (1993) concluded that uncertainties due to earthquake relocation, ellipticity and mantle corrections introduced larger errors in CMB topography than the inferred amplitudes, and that smoothing of data into spherical harmonics also increased the apparent correlation between models without having any physical meaning.

Addressing some of this criticism, a number of studies performed separate inversions for topography alone and for joint volumetric-topographic inversions (Obayashi and Fukao, 1997; Vasco et al., 1999; Boschi and Dziewonski, 2000; Sze and van der Hilst, 2003; Soldati et al., 2003; Soldati and Boschi, 2005). While a discrepancy between models based on PcP or PKP/PKKP data remains present, the consensus is that lowermost mantle heterogeneity should be included in any study of CMB topography, which also tends to decrease amplitudes in the resulting models (Figures 2a and 3a). More recently, Tanaka (2010) utilised differential P4KP-PcP traveltime measurements to minimise the influence of mantle structure and improve data coverage, resulting in topography amplitudes of only 2–2.5 km. Furthermore, instead of treating velocity and topography heterogeneity separately, Soldati et al. (2012) accounted for their coupling by mantle flow in their inversions. This gives rise to a reduction in topography amplitude (Figure 2a), solving also the discrepancy between PcP and PKP data according to the authors. At the same time, topography models developed through a joint tomographic-geodynamic approach improve the fit to normal-mode data, particularly when a decrease in viscosity associated with the post-perovskite phase is included (Soldati et al., 2013). These recent contributions illustrate that novel observations, improved estimates of mantle structure and considerations of dynamic flow effects are important factors in future studies.

2.3. CMB topography constrained by normal modes

Due to the heterogeneous distribution of seismic stations and events, body-wave studies of global CMB topography will always suffer from a sampling bias, especially when a global parameterisation is employed (Stark and Hengartner, 1993). Due to the large density contrast between the core and mantle, normal modes display a large sensitivity to CMB topography. Observations of their resonance frequencies are made after large-magnitude earthquakes, which provide complementary insights into CMB topography, albeit only on the longest wavelengths, while small-scale variations are averaged out.

Li et al. (1991) were the first to consider CMB topography in their analyses of normal modes. They performed both direct inversions of normal-mode frequency spectra, as well as a two-step approach using so-called splitting function measurements, that describe the lateral frequency variations attributed to a particular normal mode. The resulting models are relatively similar (Figure 2b), showing elevated topography at the LLVPs. Although the degree 2 amplitude differs slightly (Figure 3b), both models have peak-to-peak amplitudes of 4–5 km, which are lower than most body-wave models of that time. Similar peak-to-peak topography amplitudes were found by Koelemeijer et al. (2012) in a forward-modelling analysis of lower mantle sensitive normal modes.

Few other normal-mode models of CMB topography exist, primarily including it in studies of lowermost density structure (Section 3). Noticeably is the CMB topography model by Ishii and Tromp (1999), famously known for being the first normal-mode density study. This model features much larger amplitudes than Li et al. (1991), particularly in spherical harmonic degree 4 (Figure 3b) and includes topography of an opposite amplitude at LLVP locations (Figure 2b). This results in a positive degree 2 correlation with V_S structure (Figure 3d), whereas other CMB topography models show mostly a negative correlation.

Recently, Koelemeijer et al. (2017) performed a forward modelling parameter search for both lower mantle density and CMB topography, finding consistently elevated topographies for the LLVPs, irrespective of whether they were denser or lighter (Figure 2b). Noticeably, the largest amplitudes are found around the edges of the LLVPs, with the centre showing only moderate elevation. However, the topography amplitudes depend on the density anomalies (see bottom two rows of Figure 2b). Larger amplitudes are required in the case of dense LLVPs (model KDR2017-pos), whereas lower CMB topography amplitudes are present in the case of light LLVPs (model KDR2017-neg), as also evident in Figure 3b. While the topography models KDR2017-pos and KDR2017-neg are only included to demonstrate this dependence, the corresponding density models will be discussed and analysed further in following sections.

2.4. Other constraints on CMB topography

Additional constraints on CMB topography are obtained from geoid, gravity and nutation observations. To explain gravitational field measurements, Hide and Horai (1968) invoked peak-to-peak amplitudes of 8.7 km for CMB topography up to degree 4. In addition, Hager et al. (1985) estimated that a geoid anomaly of 2–3 km corresponds to relief on the CMB

of less than 3 km, which has been used as constraint in many subsequent studies of CMB topography. The main draw-back of using geodetic data to constrain CMB topography (and density) is that knowledge of the radial (and lateral) viscosity variations in the mantle are required (e.g. Hager and Richards, 1989), which remain debated (see Rudolph et al. - this volume). In addition, Liu and Zhong (2015) showed that structures in the lowermost mantle compensate each other, leading to a zero net effect on the geoid. Whether the geoid provides constraints on deep mantle structures remains thus to be determined.

To explain the period of the free core nutation, determined in length-of-day variations by very-long-baseline-interferometry, Gwinn et al. (1986) deduced that the CMB ellipticity was 5 % larger than for an Earth in hydrostatic equilibrium. This implies a value of 490±110 m for the degree 2 zonal coefficient of CMB topography, a value that was revised by Mathews et al. (2002) to be ∼390 m. Although this provides a strong constraint, and several subsequent studies have considered it, it remains difficult to fully reconcile this value with seismological observations. By calculating the pressure torque due to topography and analysing its effect on length-of-day variations, Jault and Le Mouël (1990) also obtained estimates of odd-degree CMB topography coefficients, finding amplitudes of a few km. The importance of topographic variations for explaining length-of-day variations has been questioned in more recent studies (Kuang and Bloxham, 1997; Kuang and Chao, 2001; Mound and Buffett, 2005), with a gravitational coupling mechanism currently favoured (see Buffett, 2015, for an discussion). Nevertheless, gravitational coupling remains dependent on flow-induced deformation of the CMB (Mound and Buffett, 2006), while small-scale roughness is still thought to influence frictional dissipation at the CMB (Le Mouël et al., 2006). Due to their complementary nature to seismological data, gravity, geoid and nutation observations will be able to contribute important constraints on CMB topography in future studies, particularly with more precise observations available (Cesare and Sechi, 2013; Bacchetta et al., 2017; Ros et al., 2018; Gurvits, 2019).

2.5. Dynamic predictions of CMB topography

Before reviewing the density structure of the lowermost mantle, first a few remarks on geodynamic predictions of CMB topography. The correlation of the non-hydrostatic geoid (Hager et al., 1985; Hager and Richards, 1989) and large-scale plate motions (Forte and Peltier, 1987) with lower mantle structure was recognised early on. As a result, geodynamic predictions of density structure and CMB topography have been compared to

seismological models with the aim to unravel the contribution of thermal and compositional variations and to further our understanding of lower mantle dynamics. Excellent reviews on these topics are given by Forte (2007) and Deschamps et al. (2018), and thus only summarised briefly here.

Dynamic predictions of CMB topography generally take one of two possible approaches. Often, seismic velocity variations are converted to density variations (generally using a scaling factor), which drive mantle flow and lead to dynamically induced CMB topography (e.g. Forte et al., 1995; Forte, 2007; Steinberger and Holme, 2008). Although the resulting models show a strong correlation with seismic tomography, several assumptions regarding the velocity-density scaling factors and viscosity structure of the mantle affect the results. An alternative approach is the modelling of mantle flow over time and analysing the present-day dynamic topography (e.g. Yoshida, 2008; Lassak et al., 2010; Liu and Zhong, 2015; Deschamps et al., 2018). Interestingly, Liu and Zhong (2015) found that the largest topography amplitudes may occur outside the LLVPs on relatively short wavelengths, while the CMB underneath the LLVPs is relatively smooth and only slightly depressed or elevated. By investigating both purely thermal and thermochemical models, Lassak et al. (2010) found that it is difficult to distinguish between the two based on long-wavelength patterns of topography up to spherical harmonic degree 4, precisely what most seismological studies have been able to constrain. However, more recent work by Deschamps et al. (2018) suggests that the relationship between S-wave velocity and CMB topography may also hold clues to the density structure of the lower mantle, even if the lowermost mantle post-perovskite phase is included (Deschamps and Li, 2019). These studies serve thus as useful guide in the interpretation of seismological results, but, as they are not derived from observations, are not of focus here.

3. Twenty years of density models

Most studies of lowermost density have focused on the nature of the LLVPs by considering the relationship between density and V_S variations. Although geodetic observations provide some constraints on density variations, on long wavelengths it is difficult to pinpoint anomalies in depth, while knowledge of the mantle's viscosity structure is generally required. Studies that utilise seismic tomography are dependent on conversion factors from velocity to density (e.g. Forte et al., 1995; Simmons et al., 2009), which tend to have large uncertainties. Here, the focus is instead on constraints from normal modes, which are thought to provide the most direct estimates of

density . Nevertheless, the sensitivity of normal modes to density structure is smaller than the sensitivity to velocity or topography (due to the oscillatory nature of the kernels around zero) and building a density model from normal-mode observations remains tricky, as this overview will show. I again take a historical view, discussing the first model that was developed 20 years ago and the criticism it received, as well as recent attempts in constraining the density structure of the lower mantle based on normal modes and tidal tomography. Note that these models generally provide a depth-averaged picture, as studies parameterise density in thick constant depth layers due to the broad depth sensitivity of the data. In reality however, the density structure is likely to have strong three-dimensional variations, even within the LLVPs (e.g. Mulyukova et al., 2015; Li et al., 2018).

3.1. Early normal-mode studies

The first normal-mode based density model was developed by Ishii and Tromp (1999), based on splitting function measurements up to 3 mHz (Tromp and Zanzerkia, 1995; He and Tromp, 1996; Resovsky and Ritzwoller, 1998). The dense LLVPs and their negative correlation with V_S structure (Figures 2c and 3f) that characterised this model had a large impact on the deep Earth community, given they could not be explained by purely thermal variations. The implication that the LLVPs were chemically distinct and long-term stable due to their higher density provided geochemists with a possible primordial reservoir in the mantle, prompting a range of studies modelling thermochemical LLVPs (e.g. Tackley, 2002; McNamara and Zhong, 2004, 2005; Tan and Gurnis, 2005).

This model immediately prompted a number of critical studies: Resovsky and Ritzwoller (1999) argued that the results were dependent on regularisation, while both Masters et al. (2000b) and Romanowicz (2001) illustrated that the available data could not distinguish between different density scenarios. In addition, no clear correlation (positive or negative) is observed between CMB topography and density, which are expected to be dynamically related. However, subsequent studies of the same authors (Ishii and Tromp, 2001, 2004) again found dense LLVPs using different methodologies and parameterisations. The notion of dense LLVPs was confirmed by powerful probabilistic inversions of normal-mode data up to 3 mHz by Trampert et al. (2004) and Mosca et al. (2012), who also utilised mineral physics data to separately estimate the thermal and chemical contributions to density. Although these density models differ in pattern (Figure 2c) and show a larger degree 2 component (Figure 3c), all show a similar negative correlation with V_S structure (Figure 3f). Consequently, the debate regarding the

LLVP density structure seemed settled.

3.2. Recent studies utilising improved data sets

In the last decade, splitting function data sets have improved with measurements up to higher frequencies (Deuss et al., 2013; Koelemeijer et al., 2013). Moulik and Ekström (2016) stressed the importance of utilising multiple data sets, combining normal-mode measurements with body-wave and surface-wave data in their least-squares inversions, finding that dense anomalies in the lowermost mantle were necessary to fit their data (Figure 2c). Taking a different approach, Koelemeijer et al. (2017) instead focused on particular modes with unique sensitivity to lowermost mantle structure, so-called CMB Stoneley modes (Koelemeijer et al., 2013). Rather than performing a least-squares inversion, they performed a model space search of scaling factors with S-wave velocity. Their results showed two model classes, which have a similar degree 2 amplitude (Figures 2c and 3c), but are characterised by either dense (KDR2017-pos) or light (KDR2017-neg) LLVPs with an opposite relationship to CMB topography (Figure 3e, see also Section 2.3). The authors favoured the models with light LLVPs and elevated topography based on geodynamic considerations, e.g. isostasy dominating on these long wavelengths. However, depending on the density contrast and viscosity structure, topography may have a more complex relationship with velocity and density structure (Deschamps et al., 2018), casting doubt on these earlier interpretations. Irrespectively, the study by Koelemeijer et al. (2017) demonstrates the strong influence of CMB topography on density models, which cannot be ignored.

All density models discussed above have been based on splitting function measurements, which are generally obtained using a self-coupling or group-coupling approximation in which a mode or group of modes is treated as isolated (Dahlen and Tromp, 1998; Deuss and Woodhouse, 2001; Al-Attar et al., 2012). Al-Attar et al. (2012) showed that these approximations are not appropriate for studies of density, as the theoretical error due to using the approximation is of similar magnitude to the density signal itself. Akbarashrafi et al. (2017) demonstrated the limitations of self-coupled splitting functions in more practical applications, but their investigations were restricted to a selection of normal modes with primary sensitivity to V_S structure. Therefore, it remains to be investigated how appropriate the self-coupling approximation is in practical studies of density studies that use higher-frequency and Stoneley modes. Fact remains nevertheless, that only even spherical harmonic degrees can be constrained while the self-coupling approximation is utilised.

3.3. New developments in density studies

A new approach to constrain the density structure of the lower mantle was introduced by Lau et al. (2015), which makes use of satellite observations of the Earth's tides. These data are very sensitive to the degree 2 structure of the deep mantle, but contain little information on higher degree structure. Although the tidal signal is modelled using normal modes, it uses full-coupling instead of the self-coupling approximation. With this tidal tomography approach, Lau et al. (2017) performed a probabilistic study, finding dense LLVPs in the deepest mantle with a range of possible scaling factors (mean model shown in Figure 2c). As the model was developed using scaling factors to S-wave tomography models, it features a strong negative correlation between density and V_S (Figure 3f). It is worth noting that the dense-LLVP model by Koelemeijer et al. (2017, KDR2017-pos), which was also built using scaling factors, has a similar negative correlation, while other studies that did not use scaling factors have smaller values. This indicates that the model parameterisation still has an important influence on current model results. Ding and Chao (2018) also deduced the presence of excess density in LLVP regions based on GPS observations and their correlation to periodic variations in the length-of-day. While these are very promising developments, certain assumptions that may influence the results (atmospheric corrections, ocean tidal loading, influence of CMB topography) still require further investigation.

The density structure of the deep mantle has been and will continue to be debated. Most studies report observations of dense LLVPs (Figure 3f), but it is unclear how much studies agree on the location of dense anomalies. In the following, I will investigate how consistent current density models are, indicate where some of the differences arise from and finally discuss ways to reconcile these in future.

4. Quantitative assessment of existing seismological models

To identify similarities and differences in models of CMB topography and density, a more quantitative analysis is required than a visual inspection of Figures 2 and 3. I take a similar approach as previous studies for finding consistent features, following the work on the SMEAN model by Becker and Boschi (2002) and the vote map approach of Shephard et al. (2017) to develop average models and vote maps of CMB topography and density. These provide complementary information on model consistency as amplitudes are included in the computation of average models (i.e. a par-

ticular model may dominate), while vote maps are only based on patterns and relative amplitudes within models themselves.

Most models considered here are long-wavelength, global models, often derived from normal-mode data and/or defined by a set of spherical harmonic coefficients. Therefore, spherical harmonics are adopted here, which also facilitates to explore just the degree 2 signal of the LLVPs. Global models are thus expanded into spherical harmonics up to degree $l = 20$ and truncated at lower degree to reduce spectral aliasing. In the following, I will use $lcut = 6$, as most models only describe heterogeneity up to $l = 4$ or $l = 6$ with not much power in higher degrees (Figure 3a–c).

Velocity and density are three-dimensional fields that vary with depth, while CMB topography only varies laterally. Given the primary interest in the relationship between CMB topography and density structure, a representative depth of 2800 km is considered only, thus treating velocity and density also as two-dimensional fields. Currently this is a justifiable choice, as most studies parameterise the density structure in thick layers of constant structure (e.g. Trampert et al., 2004; Koelemeijer et al., 2017; Lau et al., 2017), but depth variations will have to be considered when more complex seismological models become available. Furthermore, I only use lateral variations and consequently set the degree 0 coefficients to zero, with the importance of a non-zero radial average discussed in Section 5. Note that for probabilistic studies (Trampert et al., 2004; Mosca et al., 2012; Koelemeijer et al., 2017; Lau et al., 2017) only the mean models are used here even though these studies provide model uncertainties.

I consider all available global models of density and CMB topography listed in Table 1. The topography model of Creager and Jordan (1986) is excluded due to its high amplitude and the interpretation by the authors that this cannot all be due to CMB topography. In addition, multiple models from a particular study are only included if they differ significantly in their methodology; i.e. both LGW1991-SAT and LGW1991-SAF (derived from normal-mode spectra or splitting functions) and both SBF2012-T and SBF2012-TGppv (developed using a seismic or coupled seismic-geodynamic approach). However, DH1989-M7 and SBF2012-TG are not included due to their strong similarity to DH1989-M6 and SBF2012-TGppv respectively. Both model classes of Koelemeijer et al. (2017) are considered for density structure, as these models have a contrasting degree 2 component. For CMB topography, I only include KDR2017 though, as Stoneley mode data prefer this model and it has intermediate amplitudes compared to KDR2017-pos and KDR2017-neg (see Figure 2b). The final selection of models includes 10 CMB topography and 7 density models, which are indicated in bold in

Table 1.

4.1. Cross-model correlation

The similarity of any two models is calculated using the correlation between their spherical harmonic expansions. The cross-model correlation for density is mostly positive for degree 2 (Figure 4a), with the exception of model KDR2017-neg as expected. However, the correlation of Metal2012 or ME2016 with IT1999 is also visibly lower. This is likely because the extrema in density are not co-located with the LLVPs for these models, as evident from the lower correlation between V_S and density structure (Figure 3f). The correlation between Letal2017 and KDR2017-pos is very high (0.96) for degree 2, as the studies use a similar approach in which they search for optimal scaling factors with velocity. The cross-model correlation is weaker when structure up to degree 6 is considered (Figure 4b), but it remains mostly positive.

CMB topography models do not display as much consistency as density models for degree 2 structure only or all structure up to degree 6 (Figure 4c–d), particularly when body-wave models are considered (top left quadrant of the plots). In contrary, normal-mode models are generally consistent (except for IT1999) and also correlate positively with SBF2012T and SBF2012TGppv (correlation values above 0.60). Therefore, when analysing average models or vote maps, it will be important to consider body-wave and normal-mode models separately, and to bear in mind that IT1999 stands out based on the cross-model correlation.

4.2. Average models

Using insights from the previous section, I calculate average models for density and CMB topography for different selections of models. These average models should not be interpreted as tomographic models themselves, instead they act merely as useful means to condense information from a suite of models.

Including either KDR2017-neg or KDR2017-pos to calculate the average density (RMEAN_{neg} and RMEAN_{pos} in Figure 5a) makes little difference, as only one out of six models is changed. Positive densities are observed under the North Pacific and Southern Africa (the rough locations of the LLVPs), as well as under Indonesia and South America (where subducted material may be present), while negative anomalies are mainly found under the Indian Ocean and the poles. Due to inconsistencies between KDR2017-neg and the other models included, RMEAN_{neg} shows more small-scale variations

compared to RMEAN$_{pos}$. Overall, observed amplitudes are reasonable (0.2–0.3 times V_S amplitudes), with maximum amplitudes of 0.6 % relative to the radial average.

For CMB topography, average models based on normal-mode, body-wave data or both, show similar amplitudes up to ∼2.5 km, which is within the range suggested by Koelemeijer et al. (2012). There is a disparity between models based on normal modes (that show a ring of elevated topography around the North Pacific and Southern Africa) and those based on body waves (where the peaks in elevated topography are shifted - i.e. located more south in the Pacific and more north under Europe). TMEAN$_{modes}$ features an interesting gap of depressed topography under Southern Africa and the North Pacific. Before this feature is interpreted, it should be noted that IT1999 model differs from other models in having a large negative amplitude at these locations (see Figure 2b). TMEAN$_{body}$ also shows hints of depressed topography under Southern Africa and contains a pronounced area of elevated topography under Northwestern Africa, which is observed in a few individual models as well.

4.3. Vote maps of density and CMB topography

Following Shephard et al. (2017), I calculate vote maps of density and CMB topography using the same model selections. In constructing vote maps, only model amplitudes above a particular threshold are considered, which are assigned a unit vote. These are subsequently summed together for a particular selection of models (Shephard et al., 2017). Vote maps based on a positive mean (Figure 5b) allows the identification of higher density anomalies and elevated topography. I also visualise 'combined' vote maps in which vote maps based on a positive and negative mean are combined (Figure 5c), so that they can be more readily compared to average models (Figure 5a). Note that these vote maps do not serve to replace tomographic models, but merely serve to identify consistent model features.

For density, high vote locations are consistent with the average models, e.g. positive densities under the North Pacific and Southern Africa and negative anomalies under the Indian Ocean and the Poles, with the addition of the East Pacific. The vote count increases when KDR2017-pos is included instead of KDR2017-neg, although this is more evident for degree 2 structure only. The strong similarity between RMEAN and RCOMBI implies that no particular model is dominating the results and that there is large consistency between models. This allows locating the most robust dense anomalies, identified below Southern Africa (centred around Angola - Namibia) and in the North Pacific (close to Hawaii).

For CMB topography, normal-mode models (TVOTE_{modes}) show strong agreement on the location of elevated topography in the central Pacific and central Africa, while they also agree on the location of depressions under Australia and Central America. On the contrary, body-wave models (TVOTE_{body}) show less agreement, evidenced by a lower vote number, but several of these models indicate elevated topography under the Pacific as well. The vote maps further strengthen the notion of a disparity between normal-mode and body-wave models, with a shift in the location of elevated topography. The low vote count in TVOTE_{all} and TCOMBI_{all} reflects this disagreement, which needs to be resolved in future studies.

Finally, the disagreement between TMEAN and TCOMBI models raises the suspicion that average models are dominated by particular models, likely MD1987 and IT1999, which have large amplitudes and are poorly correlated to other topography models (Figure 4). The distinct ring of elevated topography in TMEAN_{modes}, which coincides with the location of high density anomalies, is not present in TVOTE_{modes} and TCOMBI_{modes}. This implies that this is due solely to poor agreement between IT1999 and other models. This serves as a reminder why average models should be treated with care and why vote maps may be more reliable for finding consistent features, even though they do not provide amplitude information.

4.4. Comparison to geodynamic predictions

As mentioned in Section 2.5, Deschamps et al. (2018) suggested that the correlation between V_S and CMB topography provides constraints on the density structure of the lowermost mantle. This study thus provides seismologists a simple metric to compare results to without necessarily having constraints on the density structure. Of course, this is only one way of comparing geodynamic predictions with seismology, and the results will inevitably be dependent on the parameters and assumptions of the geodynamic simulations (e.g. Rayleigh number, viscosity structure, mineral physics conversions), which may particularly impact the resulting topography amplitudes and implied chemical density difference. Nevertheless, if we are to make progress in constraining deep mantle structures, such simple metrics and comparisons will be crucial.

For purely thermal (TH) models, mantle flow enhances isostatic topography so that plumes cause positive topography, while increased temperatures lead to slower seismic velocity variations. Consequently, a negative V_S-topography correlation is expected. For thermochemical models (TC), an increased intrinsic density depresses the boundary through isostatic compensation, which is balanced by flow-induced dynamic topography (as hotter

piles tend to rise, stretching the CMB upwards and strongly reducing the depression due to their weight). The net effect depends on the density difference between thermochemical piles and the surrounding mantle and the wavelengths we are considering. On long wavelengths, due to a smoothing effect, small-scale variations will be averaged out, even when the largest topography amplitudes may be outside the piles. Deschamps et al. (2018) find that for a density difference $\delta\rho_C < 100kg/m^3$ (weakly thermochemical), the long-wavelength topography component is positive beneath piles leading to an anti-correlation with V_S anomalies. On the contrary, for a large density contrast $\delta\rho_C > 100kg/m^3$ (strongly thermochemical models), hot iron-enriched piles depress the CMB and have slow seismic velocities, so that V_S anomalies and CMB topography are strongly correlated. While uncertainties in thermal viscosity contrast and the presence of post-perovskite influence the topography-velocity relationships, Deschamps et al. (2018) and Deschamps and Li (2019) mapped out the ranges of resulting possibilities, which are shown in Figure 6. These predictions are compared to the seismological models presented here, considering both the V_S-topography correlation and peak-to-peak amplitudes of CMB topography. Note that this correlation is only computed for one particular depth, while the structures in the Earth are expected to vary with depth as well.

Most seismological models feature a peak-to-peak CMB topography below 4.7 km for degree 2 (Figure 6a), with the exception of IT1999, a model that shows poor consistency to others (Figure 2 and 4). These amplitudes can be reproduced by a range of geodynamic scenarios, including TH, weakly-TC and strongly-TC models. A larger range is found for structures up to degree 4 (Figure 6b), with amplitudes up to ∼12 km (excluding IT1999). However, if only models since 2000 are considered, which have utilised more recent mantle models for velocity corrections, only amplitudes up to ∼7 km are found. Irrespective of which models are considered, several geodynamic scenarios produce similar values, leading to the same conclusion as previous studies (Lassak et al., 2010; Deschamps et al., 2018); that peak-to-peak topography amplitudes cannot discriminate between thermal and thermochemical structures. Note however, that for structures up to degree 4, seismological models tend to show smaller amplitudes than those predicted, particularly for normal-mode based models, although the predicted amplitudes may be overestimates depending on the Rayleigh number of the simulations (Liu and Zhong, 2015).

The correlation between velocity and CMB topography is mostly negative or close to zero, although it spans a wide range (Figure 6c). Considering only models that demonstrated consistency in the cross-model correlation

(Figure 4), the V_S-topography correlation is lower than -0.4, which would rule out strongly-TC models with $\delta\rho_C > 100$ kg/m^3 (though the exact value will depend on the Rayleigh number of the simulations). While this inference is based mostly on models derived from normal-mode data, these have the advantage that they provide global coverage, have a clear sensitivity to CMB topography and make fewer approximations in the theoretical treatment. In addition, several body-wave models show similar relationships, for example, Soldati et al. (2003) found a strong negative correlation in their joint inversions of CMB topography and velocity. The V_S-topography correlation for the average (MEAN) and vote map (COMBI) models of Figure 5 supports this notion, with values of -0.52 and -0.75 respectively. These values only fall within the range of geodynamic predictions for TH or weakly-TC models with a large thermal viscosity contrast, with or without post-perovskite, suggesting that strongly thermochemical models are inconsistent with seismological constraints on CMB topography. However, current models still span a wide range in peak-to-peak amplitudes and correlation values, preventing us from drawing more decisive conclusions regarding the state of the lower mantle. Naturally, these inferences will require reconsideration when improved seismological models of CMB topography become available.

4.5. Summary of current model features

A number of inferences can be drawn from the average models and vote maps of lower mantle density structure and CMB topography introduced here:

- For density, average models and vote maps consistently identify two areas of dense anomalies; one located below Southern Africa (centred around Angola), roughly in the core of the LLVP imaged in seismic velocity. The other one is found under the North Pacific (close to Hawaii), located more on the edge of the LLVP as imaged in seismic velocity.

- Considering both model classes of Koelemeijer et al. (2017) allows to resolve recent results based on Stoneley modes and tidal measurements (Lau et al., 2017). The cross-model correlation between Letal2017 and KDR2017-pos is particularly high (0.96 for degree 2) as the two studies employ a similar scaling to velocity.

- Topography models mostly show elevated topographies under the Pacific and Africa, but details differ between average models and vote maps. All models have a peak-to-peak amplitude below 4.7 km for

degree 2, with the exception of the IT1999 model, that also appears inconsistent with other normal-mode models.

- A discrepancy is observed between body-wave and normal-mode models of CMB topography, with normal-mode models showing a stronger relationship with velocity structure.
- The correlation between current models of CMB topography and V_S shows a range of values, but tends to be mostly negative.
- Although unique interpretations are difficult, a comparison with recent work by Deschamps et al. (2018) suggests that strongly thermochemical models are inconsistent with current seismological models.

The fact that the studies of Koelemeijer et al. (2017) and Lau et al. (2017) can be reconciled when a different relationship to CMB topography is adopted is a step forward to building consistent models of the deep mantle. It will thus be crucial to develop robust models of CMB topography that are compatible with a range of data: reflected and refracted body waves, normal modes and geodetic data, in addition to developing improved density models.

5. Efforts towards more consistent models

Here, I first discuss several factors that I believe are important to consider when interpreting density models, followed by suggestions for the future development of consistent density and CMB topography models.

5.1. Factors influencing the interpretation of density models

In visualisations of seismic models, we tend to plot lateral variations with respect to a radial average, which may be significantly different from zero. Particularly, several normal-mode studies have found a positive density in the lowest 150–500 km of the mantle compared to the PREM model (Dziewonski and Anderson, 1981), ranging in amplitude between 0.1 % and 0.6 % (Montagner and Kennett, 1996; Masters and Gubbins, 2003; De Wit et al., 2014). When thinking about the buoyancy of the LLVPs, these constraints on the radial density structure should be integrated in interpretations. It also remains important to consider the dynamic implications of density variations in regions surrounding the LLVPs, e.g. if these constitute of colder, subducted slabs, we may expect them to be denser. Furthermore, the LLVPs are likely very three-dimensional structures, with possibly near

neutral buoyancy and density variations within (Mulyukova et al., 2015; Li et al., 2018). Current density models that often have thick constant layers should thus be interpreted with caution as they represent depth averages of complex structures.

Unravelling the relative importance of thermal and chemical contributions to density as imaged in tomography is not straightforward. Advances in mineral physics will have to be made to reduce uncertainties in partial derivatives that are needed to relate variations in temperature and chemical composition to seismic velocity and density. Another difficulty in interpreting density results arises when models provide a range of possibilities (Koelemeijer et al., 2017; Lau et al., 2017) or a mean model with uncertainties (Trampert et al., 2004; Mosca et al., 2012). These approaches are very powerful and clearly the way forward, especially when combining multiple data sets with different sensitivities. In such probabilistic studies, care should be taken in communicating the results to ensure that both the model and the uncertainties are fully exploited in subsequent work.

We should also consider the effect that the transition from bridgmanite to post-perovskite (∼0.5–1.5 % increase in density (Murakami et al., 2004; Oganov and Ono, 2004; Tsuchiya et al., 2004; Cobden et al., 2015)) may have on our interpretations. Even if post-perovskite is only present in colder (fast-velocity) regions, this will affect the radial average at those depths, which leads to a bias in interpretations of lateral variations (Styles et al., 2011). In addition, the presence of weak pPv will influence lower mantle dynamics and alter the relationships between velocity, density and CMB topography (Deschamps and Li, 2019).

Finally, we tend to think of the African and Pacific LLVP as two of the same kind. This is partly because many older V_S models (and most density models) utilised normal-mode data that only provided even-degree constraints, thus resulting in an inherent symmetry. However, such an even-degree expansion may no longer be warranted, given that density anomalies change from positive to negative within the Pacific LLVP, while they are co-located for the African LLVP (Figure 5). In addition, V_S and V_P anomalies show a consistent pattern for the African LLVP, but the extrema seem shifted with respect to each other for the Pacific LLVP (Figure 1). This suggests that the Pacific anomaly locations are not as well constrained as under Africa, with possible artefacts due to the even-degree expansion of the data and models. In interpreting these anomalies, it is thus important to always verify that the relationships between velocity, density and topography are consistent with our understanding of mineral physics and mantle dynamic processes. To improve our understanding of lower mantle dynam-

ics, we may have to move away from even-degree expansions and consider different explanations for the African and Pacific LLVP.

5.2. Future development of density models

Several avenues can be followed to improve density models and reconcile present model differences, both in terms of theory and methodology.

Most importantly, to reduce theoretical errors (Al-Attar et al., 2012), it is crucial to perform direct spectral inversions using full-coupling instead of using self-coupled splitting function measurements. Ideally, in order to reconcile differences with current models, the results of such spectral inversions will be compared to models developed using self-coupled splitting functions based on the same spectra, similar to Li et al. (1991). At the same time, the robustness of current self- and group-coupled splitting function measurements (particularly Stoneley modes) should be assessed, similar to has been done for a selection of V_S- and V_P- sensitive modes (Akbarashrafi et al., 2017). An increased availability of geodetic data will enable more detailed tidal tomography studies, which provide independent constraints on density. By combining insights and constraints from such different data sets (including gravity), future studies should be able to resolve the trade-off between density and CMB topography and narrow down the available parameter space.

Past studies have taken different approaches to solving the inverse problem, mostly adopting a least-squares inversion (e.g. Ishii and Tromp, 1999; Moulik and Ekström, 2016) or performing probabilistic model space searches (e.g. Trampert et al., 2004; Mosca et al., 2012; Koelemeijer et al., 2017; Lau et al., 2017). The data sets utilised in these studies differ in quantity, quality and type; older studies only had normal-mode data up to 3 mHz available (Ishii and Tromp, 1999; Trampert et al., 2004), while recent studies have focused on different normal modes that vary in their sensitivity to density. Moulik and Ekström (2016) emphasised the importance of mode ${}_0S_2$, Koelemeijer et al. (2017) focused their analysis on CMB Stoneley modes, while Lau et al. (2017) include 16 modes in their modelling. Understanding the implications of these subjective choices and testing their effect in future inversions, ideally through comprehensive studies in which different mode selections, data uncertainties and inverse techniques are compared, will be important to reconcile current differences.

Choices regarding the vertical and lateral parameterisation should also be carefully considered. A finer depth parameterisation than in previous studies has to be incorporated to find out the depth extent of any dense material within the LLVPs - e.g. whether it is confined to a thin layer at the

bottom or several hundreds kilometres thick (Romanowicz, 2017). As the density structure is likely to have strong three-dimensional variations, it will be important to determine which parts of the LLVPs (if any) are neutrally buoyant (Mulyukova et al., 2015; Li et al., 2018). The choice of lateral parameterisation also influences inversion results (discussed in Section 4), while it should be remembered that global correlation values are not just affected by the LLVPs. Particularly, the scaling of density to velocity may results in unrealistic scenarios; if the lowest velocities in the centre of the LLVPs represent the highest temperatures, we would expect an overall zero density anomaly instead of finding the strongest density anomalies in the centre as well. In such a scenario, even though the strongest anomalies are found near the edges of the LLVPs, the degree 2 component may still show a higher density, which is compensated by higher degree structure (as is the case for the KDR2017pos density model).

Finally, unmodelled complexities (e.g. anisotropy, discontinuity topography, source complexity, scattering and focusing effects) should also be considered in future inversions, as these trade-off with density (Moulik and Ekström, 2016). Particularly, the work by Koelemeijer et al. (2017) and earlier results from Koelemeijer et al. (2012) demonstrate the strong trade-offs between CMB topography and density structure. Including CMB topography in future inversion for density will not only help to reconcile current models, but also aid in distinguishing different dynamic scenarios by analysing the relationship of CMB topography and velocity.

5.3. Developing consistent CMB topography models

Seismological inferences of CMB topography will always be complicated by trade-offs with lower mantle and outermost core structure. Particularly for PmKP waves and Stoneley modes, it will be important to consider the possibility of both radial and lateral structures at the top of the outer core. Ideally, studies should study the two boundary regions of CMB together instead of treating them separately. Such efforts will also aid in reconciling inferences from body-wave and normal-mode data.

Instead of ray theory, body-wave studies should make use of finite-frequency theory including joint volumetric and topographic kernels (Colombi et al., 2014). The choice of phases in these endeavours will be important, as reflected phases will provide good constraints on short-scale structure and amplitudes, while diffracted phases will aid in constraining long-wavelength structures and patterns (Colombi et al., 2012). Differential measurements of exotic phases (e.g. PK4P-P or PK7P-PK4P) form useful complementary data, but complicate interpretation due to their multiple bounce points.

Similar to studies of dynamic surface topography (see Austermann & Hoggard, this volume), care should be taken when laterally expanding body-wave data to prevent spurious amplitudes (Pulliam and Stark, 1993) and an apparent consistency between models (Stark and Hengartner, 1993).

Normal modes have an important role to play in constraining long-wavelength topographic variations. Current available data sets of splitting function measurements have not yet been fully exploited and can be used to develop improved normal-mode based models. Although the treatment of lower mantle density structure should be an important consideration in such studies, Koelemeijer et al. (2017) demonstrate that relatively consistent CMB topography models are obtained independently of density. In addition, improved normal-mode models of CMB topography may provide additional constraints on lower mantle density (Deschamps et al., 2018), warranting intensified efforts.

Ideally, body-wave and normal-mode data are exploited together to build a consistent model of CMB topography, either through joint inversions or combined model space searches. In these studies, it will be crucial to address differences in length scales and to perform joint inversions of CMB topography and structure in the lower mantle and outermost core. If the largest topography amplitudes are on the side of or outside the LLVPs (Liu and Zhong, 2015), normal modes would provide a smooth representation of this topography, which should be combined with spot measurements using body waves to find these extreme topography amplitudes (similar to Wu et al., 2014). Such a focus on specific regions with good data coverage will also enable the use of appropriate theory for the treatment of body-wave data. With advances in computing power and data coverage, it may be possible in future to expand such an approach to the entire surface of the CMB.

5.4. Integrating seismology with other constraints

In this contribution, I have quantitatively compared seismological models with insights from geodynamics, utilising the correlation between velocity and CMB topography as suggested by Deschamps et al. (2018). While the results of these comparisons (e.g. the maximum $\delta\rho_C$) will be dependent on the parameters of the geodynamic simulations and approximations, such a simple metric provides seismologists a powerful tool to compare observations to. Naturally, when new seismological models are available, other inferences may be drawn.

In future studies, it will be crucial to integrate geodetic data and insights from geodynamics with seismological observations. In order to achieve this, improved estimates of mantle viscosity as well as smaller uncertainties in

mineral physics will be required. Especially, obtaining a sufficient fit to the geoid as well as satisfying constraints on excess ellipticity from nutation data at the same time as seismological data will be a challenge. Therefore, it would be best to take a probabilistic approach so that the different data uncertainties can be included. This will likely be the only way to make substantial progress in studies of lower mantle density and CMB topography.

6. Conclusions

Robust models of lower mantle density and CMB topography provide vital information on mantle upwellings and dynamics. Despite studies spanning several decades, models still lack consistency in both pattern and amplitude. Most density models find two areas of dense anomalies roughly co-located with the LLVPs imaged in S- and P-wave velocity models, but details vary and the effect of CMB topography on the retrieved density structure requires more investigation. Current models of CMB topography differ in their patterns but generally feature elevated topography at LLVP locations and most have a degree 2 peak-to-peak amplitude below 4.7 km.

Lower mantle models of S-wave and P-wave velocity have converged more and more in the last ten years, so how do we achieve the same for models of lower mantle density and CMB topography? Future studies of density should not only utilise improved normal mode theory and the advances in computation power, but also investigate the effects of subjective choices (e.g. data, parameterisation) and combine several seismological and geodetic data types to break trade-offs with CMB topography. Simultaneously, efforts to obtain independent constraints on CMB topography should be intensified, particularly with the aim to develop models that are consistent with both body-wave and normal-mode data across a range of wavelengths. Such consistent models of the seismological landscape of the CMB will not only provide insights into lowermost mantle dynamics, but also be important for studies of outer core flow, inner core structure and evolution.

Acknowledgements

The author thanks the Associate Editor (Sanne Cottaar), Satoru Tanaka and two anonymous reviewers for their constructive comments, which have improved this manuscript. The author is funded by a Royal Society University Research Fellowship (URF\R1\180377) and gratefully acknowledges their support. This work has also received support from a Junior Research Fellowship awarded by University College, Oxford. The author is grateful to

Ed Garnero, Frédéric Deschamps, Jeff Winterbourne, Jeroen Ritsema, Arwen Deuss, Harriet Lau and Raj Moulik for stimulating discussions. Thanks also to all authors of CMB topography, velocity and density models for sharing their models and insights. Figures have been produced using the Generic Mapping Tools (GMT) version 5 software (Wessel et al., 2013).

References

Akbarashrafi, F., Al-Attar, D., Deuss, A., Trampert, J., Valentine, A., 2017. Exact free oscillation spectra, splitting functions and the resolvability of Earth's density structure. Geophys. J. Int. 213 (1), 58–76.

Al-Attar, D., Woodhouse, J., Deuss, A., 2012. Calculation of normal mode spectra in laterally heterogeneous Earth models using an iterative direct solution method. Geophysical Journal International 189 (2), 1038–1046.

Aleshin, H., Vinnik, L., 1975. The topography of the core-mantle interface. Bull. Acad. Sci. USSR, Phys. Solid Earth 11 (7).

Asari, S., Shimizu, H., Utada, H., 2006. Variability of the topographic core-mantle torque calculated from core surface flow models. Phys. Earth Planet. Inter. 154 (1), 85–111.

Auer, L., Boschi, L., Becker, T., Nissen-Meyer, T., Giardini, D., 2014. Savani: A variable resolution whole-mantle model of anisotropic shear velocity variations based on multiple data sets. J. Geophys. Res. 119 (4), 3006–3034.

Austermann, J., Kaye, B. T., Mitrovica, J. X., Huybers, P., 2014. A statistical analysis of the correlation between large igneous provinces and lower mantle seismic structure. Geophys. J. Int. 197 (1), 1–9.

Bacchetta, A., Colangelo, L., Canuto, E., Dionisio, S., Massotti, L., Novara, C., Parisch, M., Silvestrin, P., 2017. From GOCE to NGGM: Automatic Control Breakthroughs for European future Gravity Missions. IFAC-PapersOnLine 50 (1), 6428–6433.

Bataille, K., Flatté, S. M., 1988. Inhomogeneities near the core-mantle boundary inferred from short-period scattered PKP waves recorded at the global digital seismograph network. J. Geophys. Res. 93 (B12), 15057–15064.

Bataille, K., Wu, R., Flatte, S., 1990. Inhomogeneities near the core-mantle boundary evidenced from scattered waves: A review. Pure Appl. Geophys. 132 (1-2), 151–173.

Becker, T., Boschi, L., 2002. A comparison of tomographic and geodynamic mantle models. Geophys. Geochem. Geosys. 3 (1), 1003.

Boschi, L., Dziewonski, A. M., 2000. Whole Earth tomography from delay times of P, PcP, and PKP phases: Lateral heterogeneities in the outer core or radial anisotropy in the mantle? J. Geophys. Res. 105 (B6), 13675–13696.

Bower, D. J., Gurnis, M., Seton, M., 2013. Lower mantle structure from paleogeographically constrained dynamic Earth models. Geophys. Geochem. Geosys. 14 (1), 44–63.

Buffett, B., 2015. Core-mantle interactions. In: Schubert, G. (Ed.), Treatise on Geophysics . Vol. 8. Elsevier, pp. 213–224.

Burdick, S., Vernon, F. L., Martynov, V., Eakins, J., Cox, T., Tytell, J., Mulder, T., White, M. C., Astiz, L., Pavlis, G. L., et al., 2017. Model update May 2016: Upper-mantle heterogeneity beneath North America from travel-time tomography with global and USArray data. Seism. Res. Lett. 88 (2A), 319–325.

Burke, K., Steinberger, B., Torsvik, T. H., Smethurst, M. A., 2008. Plume generation zones at the margins of large low shear velocity provinces on the core–mantle boundary. Earth and Planetary Science Letters 265 (1), 49–60.

Calkins, M. A., Noir, J., Eldredge, J. D., Aurnou, J. M., 2012. The effects of boundary topography on convection in Earth's core. Geophys. J. Int. 189 (2), 799–814.

Cesare, S., Sechi, G., 2013. Next generation gravity mission. In: Distributed Space Missions for Earth System Monitoring. Springer, pp. 575–598.

Chang, A. C., Cleary, J. R., 1978. Precursors to PKKP. Bull. Seismol. Soc. Am. 68 (4), 1059–1079.

Chang, A. C., Cleary, J. R., 1981. Scattered PKKP: Further evidence for scattering at a rough core-mantle boundary. Phys. Earth Planet. Inter. 24 (1), 15–29.

Chang, S.-J., Ferreira, A. M., Ritsema, J., Heijst, H. J., Woodhouse, J. H., 2015. Joint inversion for global isotropic and radially anisotropic mantle structure including crustal thickness perturbations. Journal of Geophysical Research: Solid Earth.

Cleary, J., Haddon, R., 1972. Seismic wave scattering near the core-mantle boundary: a new interpretation of precursors to PKP. Nature 240 (5383), 549.

Cobden, L., Thomas, C., Trampert, J., 2015. Seismic detection of post-perovskite inside the Earth. In: Khan, A., Deschamps, F. (Eds.), The Earth's heterogeneous mantle. Springer, pp. 391–440.

Colombi, A., Nissen-Meyer, T., Boschi, L., Giardini, D., 2012. Seismic waveform sensitivity to global boundary topography. Geophys. J. Int. 191 (2), 832–848.

Colombi, A., Nissen-Meyer, T., Boschi, L., Giardini, D., 2014. Seismic waveform inversion for core–mantle boundary topography. Geophys. J. Int. 198 (1), 55–71.

Cottaar, S., Lekic, V., 2016. Morphology of seismically slow lower-mantle structures. Geophys. J. Int. 207 (2), 1122–1136.

Creager, K., Jordan, T., 1986. Aspherical structure of the core-mantle boundary from PKP travel times. Geophys. Res. Lett. 13 (13), 1497–1500.

Dahlen, F., Tromp, J., 1998. Theoretical global seismology. Princeton University Press.

Davies, C. J., Stegman, D. R., Dumberry, M., 2014. The strength of gravitational core-mantle coupling. Geophys. Res. Lett. 41 (11), 3786–3792.

Davies, D., Goes, S., Sambridge, M., 2015a. On the relationship between volcanic hotspot locations, the reconstructed eruption sites of large igneous provinces and deep mantle seismic structure. Earth Planet. Sci. Lett. 411, 121–130.

Davies, D. R., Goes, S., Davies, J. H., Schuberth, B. S. A., Bunge, H., Ritsema, J., 2012. Reconciling dynamic and seismic models of Earth's lower mantle: The dominant role of thermal heterogeneity. Earth Planet. Sci. Lett. 353, 253–269.

Davies, D. R., Goes, S., Lau, H. C. P., 2015b. Thermally Dominated Deep Mantle LLSVPs: A Review. In: Khan, A., Deschamps, F. (Eds.), The Earth's Heterogeneous Mantle. Springer International Publishing, pp. 441–477.

De Wit, R., Käufl, P., Valentine, A., Trampert, J., 2014. Bayesian inversion of free oscillations for Earth's radial (an) elastic structure. Phys. Earth Planet. Inter. 237, 1–17.

Dehant, V., Laguerre, R., Rekier, J., Rivoldini, A., Triana, S. A., Trinh, A., Van Hoolst, T., Zhu, P., 2017. Understanding the effects of the core on the nutation of the Earth. Geodesy and Geodynamics 8 (6), 389–395.

Deschamps, F., Kaminski, E., Tackley, P. J., 2011. A deep mantle origin for the primitive signature of ocean island basalt. Nature Geosci. 4 (12), 879.

Deschamps, F., Li, Y., 2019. Core-mantle boundary dynamic topography: influence of post-perovskite viscosity. J. Geophys. Res. , 9247–9264.

Deschamps, F., Rogister, Y., Tackley, P. J., 2018. Constraints on core–mantle boundary topography from models of thermal and thermochemical convection. Geophys. J. Int. 212 (1), 164–188.

Deschamps, F., Trampert, J., 2003. Mantle tomography and its relation to temperature and composition. Phys. Earth Planet. Inter. 140 (4), 277–291.

Deuss, A., Ritsema, J., van Heijst, H.-J., 2013. A new catalogue of normal-mode splitting function measurements up to 10 mHz. Geophys. J. Int. 192 (3), 920–937.

Deuss, A., Woodhouse, J., 2001. Theoretical free-oscillation spectra: the importance of wide band coupling. Geophys. J. Int. 146 (3), 833–842.

Ding, H., Chao, B. F., 2018. A 6-year westward rotary motion in the Earth: Detection and possible MICG coupling mechanism. Earth Planet. Sci. Lett. 495, 50–55.

Doornbos, D., 1974. Seismic wave scattering near caustics: Observations of PKKP precursors. Nature 247 (5440), 352.

Doornbos, D., 1976. Characteristics of lower mantle inhomogeneities from scattered waves. Geophys. J. Int. 44 (2), 447–470.

Doornbos, D., 1978. On seismic-wave scattering by a rough core-mantle boundary. Geophys. J. Int. 53 (3), 643–662.

Doornbos, D., 1980. The effect of a rough core-mantle boundary on PKKP. Phys. Earth Planet. Inter. 21 (4), 351–358.

Doornbos, D., Hilton, T., 1989. Models of the core-mantle boundary and the travel times of internally reflected core phases. J. Geophys. Res. 94 (B11), 15741–15751.

Doornbos, D., Vlaar, N., 1973. Regions of seismic wave scattering in the Earth's mantle and precursors to PKP. Nature Phys. Sci. 243 (126), 58.

Durand, S., Debayle, E., Ricard, Y., Zaroli, C., Lambotte, S., 2017. Confirmation of a change in the global shear velocity pattern at around 1000 km depth. Geophys. J. Int. 211 (3), 1628–1639.

Dziewonski, A., Anderson, D., 1981. Preliminary reference Earth model. Phys. Earth Planet. Inter. 25 (4), 297–356.

Dziewonski, A. M., Lekić, V., Romanowicz, B. A., 2010. Mantle anchor structure: An argument for bottom up tectonics. Earth Planet. Sci. Lett. 299 (1), 69–79.

Earle, P. S., Shearer, P. M., 1998. Observations of high-frequency scattered energy associated with the core phase PKKP. Geophys. Res. Lett. 25 (3), 405–408.

Emmerich, H., 1993. Theoretical study on the influence of CMB topography on the core reflection ScS. Phys. Earth Planet. Inter. 80 (3-4), 125–134.

Forte, A., 2007. Constraints on seismic models from other disciplines – Implications for mantle dynamics and composition. In: Dziewonski, A., Romanowicz, B. (Eds.), Treatise on Geophysics . Vol. 1. Elsevier, pp. 805–858.

Forte, A., Mitrovica, J., 2001. Deep-mantle high-viscosity flow and thermochemical structure inferred from seismic and geodynamic data. Nature 410 (6832), 1049–1056.

Forte, A., Mitrovica, J., Woodward, R., 1995. Seismic-geodynamic determination of the origin of excess ellipticity of the core-mantle boundary. Geophys. Res. Lett. 22 (9), 1013–1016.

Forte, A., Peltier, W., 1987. Surface plate kinematics and mantle convection. In: Fuchs, K., Froidevaux, C. (Eds.), Composition, Structure and Dynamics of the Lithosphere-Asthenosphere System. Vol. 16. Wiley Online Library, pp. 125–136.

Forte, A. M., Peltier, W. R., 1991. Mantle convection and core-mantle boundary topography: explanations and implications. Tectonophysics 187 (1-3), 91–116.

French, S., Romanowicz, B., 2014. Whole-mantle radially anisotropic shear velocity structure from spectral-element waveform tomography. Geophys. J. Int. 199 (3), 1303–1327.

Garcia, R., Souriau, A., 2000. Amplitude of the core-mantle boundary topography estimated by stochastic analysis of core phases. Phys. Earth Planet. Inter. 117, 345–359.

Garnero, E., McNamara, A., 2008. Structure and dynamics of Earth's lower mantle. Science 320 (5876), 626.

Garnero, E., McNamara, A., Shim, S.-H., 2016. Continent-sized anomalous zones with low seismic velocity at the base of Earth's mantle. Nature Geosci. 9 (7), 481–489.

Gubbins, D., Richards, M., 1986. Coupling of the core dynamo and mantle: thermal or topographic. Geophys. Res. Lett. 13 (13), 1521–1524.

Gudmundsson, O., 1989. Some problems in global tomography: Modeling the core-mantle boundary and statistical analysis of travel-time data. PhD thesis, Calif. Inst. of Techn.

Gudmundsson, O., Clayton, R. W., 1991. A 2-D synthetic study of global traveltime tomography. Geophys. J. Int. 106 (1), 53–65.

Gurvits, L. I., 2019. Space VLBI: from first ideas to operational missions. Advances in Space Research.

Gwinn, C. R., Herring, T. A., Shapiro, I. I., 1986. Geodesy by radio interferometry: Studies of the forced nutations of the Earth: 2. Interpretation. J. Geophys. Res. 91 (B5), 4755–4765.

Haddon, R., 1972. Corrugations on the mantle-core boundary or transition layers between inner and outer cores? Eos Trans. AGU 53, 600.

Haddon, R., Cleary, J., 1974. Evidence for scattering of seismic PKP waves near the mantle-core boundary. Phys. Earth Planet. Inter. 8 (3), 211–234.

Hager, B., Clayton, R., Richards, M., Comer, R., Dziewonski, A., 1985. Lower mantle heterogeneity, dynamic topography and the geoid. Nature 313 (6003), 541–545.

Hager, B., Richards, M., 1989. Long-wavelength variations in Earth's geoid: physical models and dynamical implications. Phil. Trans. R. Soc. Lond. 328 (1599), 309–327.

He, X., Tromp, J., 1996. Normal-mode constraints on the structure of the Earth. J. Geophys. Res. 101 (B9), 20–053.

Hernlund, J., McNamara, A., 2015. The core–mantle boundary region. In: Schubert, G. (Ed.), Treatise on Geophysics . Vol. 7. Elsevier, pp. 461–519.

Hide, R., Clayton, R., Hager, B., Spieth, M., Voorhies, C., 1993. Topographic core-mantle coupling and fluctuations in the Earth's rotation. In: Geophys. Monograph AGU : Relating geophysical structures and processes. Vol. 76. AGU American Geophysical Union, pp. 107–107.

Hide, R., Horai, K., 1968. On the topography of the core-mantle interface. Phys. Earth Planet. Inter. 1 (5), 305–308.

Hofmann, A., 1997. Mantle geochemistry: the message from oceanic volcanism. Nature 385 (6613), 219–229.

Hosseini, K., 2016. Global multiple-frequency seismic tomography using teleseismic and core-diffracted body waves. PhD thesis, LMU Munich.

Houser, C., Masters, G., Shearer, P., Laske, G., 2008. Shear and compressional velocity models of the mantle from cluster analysis of long-period waveforms. Geophys. J. Int. 174 (1), 195–212.

Ishii, M., Tromp, J., 1999. Normal-mode and free-air gravity constraints on lateral variations in velocity and density of Earth's mantle. Science 285 (5431), 1231.

Ishii, M., Tromp, J., 2001. Even-degree lateral variations in the Earth's mantle constrained by free oscillations and the free-air gravity anomaly. Geophys. J. Int. 145 (1), 77–96.

Ishii, M., Tromp, J., 2004. Constraining large-scale mantle heterogeneity using mantle and inner-core sensitive normal modes. Phys. Earth Planet. Inter. 146 (1-2), 113–124.

Jault, D., Le Mouël, J., 1990. Core-mantle boundary shape: constraints inferred from the pressure torque acting between the core and the mantle. Geophys. J. Int. 101 (1), 233–241.

Kampfmann, W., Müller, G., 1989. PcP amplitude calculations for a core-mantle boundary with topography. Geophys. Res. Lett. 16 (7), 653–656.

Karato, S.-i., Karki, B. B., 2001. Origin of lateral variation of seismic wave velocities and density in the deep mantle. J. Geophys. Res. 106 (R10), 21771–21783.

Koelemeijer, P., Deuss, A., Ritsema, J., 2013. Observations of core-mantle boundary Stoneley modes. Geophys. Res. Lett. 40 (11), 2557–2561.

Koelemeijer, P., Deuss, A., Ritsema, J., 2017. Density structure of Earth's lowermost mantle from Stoneley mode splitting observations. Nature Comm. 8, 15241.

Koelemeijer, P., Deuss, A., Trampert, J., 2012. Normal mode sensitivity to Earth's D" layer and topography on the core–mantle boundary: what we can and cannot see. Geophys. J. Int. 190, 553–568.

Koelemeijer, P., Ritsema, J., Deuss, A., Van Heijst, H.-J., 2016. SP12RTS: a degree-12 model of shear-and compressional-wave velocity for Earth's mantle. Geophys. J. Int. 204 (2), 1024–1039.

Koelemeijer, P., Schuberth, B. S., Davies, D. R., Deuss, A., Ritsema, J., 2018. Constraints on the presence of post-perovskite in Earth's lowermost mantle from tomographic-geodynamic model comparisons. Earth Planet. Sci. Lett. 494, 226–238.

Koper, K. D., Pyle, M. L., Franks, J. M., 2003. Constraints on aspherical core structure from PKiKP-PcP differential travel times. J. Geophys. Res. 108 (B3).

Kuang, W., Bloxham, J., 1993. On the effect of boundary topography on flow in the Earth's core. Geophysical & Astrophysical Fluid Dynamics 72 (1-4), 161–195.

Kuang, W., Bloxham, J., 1997. On the dynamics of topographical core-mantle coupling. Phys. Earth Planet. Inter. 99 (3-4), 289–294.

Kuang, W., Chao, B. F., 2001. Topographic core-mantle coupling in geodynamo modeling. Geophys. Res. Lett. 28 (9), 1871–1874.

Lassak, T., McNamara, A., Garnero, E., Zhong, S., 2010. Core-mantle boundary topography as a possible constraint on lower mantle chemistry and dynamics. Earth Planet. Sci. Lett. 289, 232–241.

Lau, H. C., Mitrovica, J. X., Davis, J. L., Tromp, J., Yang, H.-Y., Al-Attar, D., 2017. Tidal tomography constrains Earth's deep-mantle buoyancy. Nature 551 (7680), 321.

Lau, H. C., Yang, H.-Y., Tromp, J., Mitrovica, J. X., Latychev, K., Al-Attar, D., 2015. A normal mode treatment of semi-diurnal body tides on an aspherical, rotating and anelastic Earth. Geophys. J. Int. 202 (2), 1392–1406.

Le Mouël, J.-L., Narteau, C., Greff-Lefftz, M., Holschneider, M., 2006. Dissipation at the core-mantle boundary on a small-scale topography. J. Geophys. Res. 111 (B4).

Lekić, V., Cottaar, S., Dziewonski, A., Romanowicz, B., 2012. Cluster analysis of global lower mantle tomography: A new class of structure and implications for chemical heterogeneity. Earth Planet. Sci. Lett. 357, 68–77.

Li, M., McNamara, A. K., Garnero, E. J., 2014. Chemical complexity of hotspots caused by cycling oceanic crust through mantle reservoirs. Nature Geosci. 7 (5), 366.

Li, M., Zhong, S., Olson, P., 2018. Linking lowermost mantle structure, core-mantle boundary heat flux and mantle plume formation. Phys. Earth Planet. Inter. 277, 10–29.

Li, X., Giardini, D., Woodhouses, J., 1991. Large-scale three-dimensional even-degree structure of the Earth from splitting of long-period normal modes. J. Geophys. Res. 96 (B1), 551–577.

Liu, X., Zhong, S., 2015. Constraining mantle viscosity structure for a thermochemical mantle using the geoid observation. Geophys. Geochem. Geosys. 17 (3), 895–913.

Loper, D. E., Lay, T., 1995. The core-mantle boundary region. J. Geophys. Res. 100 (B4), 6397–6420.

Lu, C., Grand, S. P., 2016. The effect of subducting slabs in global shear wave tomography. Geophys. J. Int. 205 (2), 1074–1085.

Mancinelli, N., Shearer, P., 2016. Scattered energy from a rough core-mantle boundary modeled by a Monte Carlo seismic particle method: Application to PKKP precursors. Geophys. Res. Lett. 43 (15), 7963–7972.

Masters, G., Gubbins, D., 2003. On the resolution of density within the Earth. Phys. Earth Planet. Inter. 140 (1-3), 159–167.

Masters, G., Laske, G., Bolton, H., Dziewonski, A., 2000a. The relative behavior of shear velocity, bulk sound speed, and compressional velocity in the mantle: Implications for chemical and thermal structure. In: Karato, S., Forte, A., Liebermann, R., Masters, G., Stixrude, L. (Eds.), Geophys. Monograph AGU : Earth's Deep Interior: Mineral Physics and Tomography From the Atomic to the Global Scale. Vol. 117. Wiley Online Library, pp. 63–87.

Masters, G., Laske, G., Gilbert, F., 2000b. Matrix autoregressive analysis of free-oscillation coupling and splitting. Geophys. J. Int. 143 (2), 478–489.

Mathews, P. M., Herring, T. A., Buffett, B. A., 2002. Modeling of nutation and precession: New nutation series for non-rigid Earth and insights into the Earth's interior. J. Geophys. Res. 107 (B4), ETG–3.

McNamara, A., Garnero, E., Rost, S., 2010. Tracking deep-mantle reservoirs with ultra-low-velocity zones. Earth Planet. Sci. Lett. 299 (1), 1–9.

McNamara, A. K., Zhong, S., 2004. Thermochemical structures within a spherical mantle: Superplumes or piles? J. Geophys. Res. 109 (B7).

McNamara, A. K., Zhong, S., 2005. Thermochemical structures beneath Africa and the Pacific Ocean. Nature 437 (7062), 1136–1139.

Menke, W., 1986. Few 2-50 km corrugations on the core-mantle boundary. Geophys. Res. Lett. 13 (13), 1501–1504.

Montagner, J., Kennett, B., 1996. How to reconcile body-wave and normal-mode reference Earth models. Geophys. J. Int. 125 (1), 229–248.

Morelli, A., Dziewonski, A., 1987. Topography of the core–mantle boundary and lateral homogeneity of the liquid core. Nature 325, 678–683.

Mosca, I., Cobden, L., Deuss, A., Ritsema, J., Trampert, J., 2012. Seismic and mineralogical structures of the lower mantle from probabilistic tomography. J. Geophys. Res. 117 (B6), B06304.

Moulik, P., Ekström, G., 2014. An anisotropic shear velocity model of the Earth's mantle using normal modes, body waves, surface waves and long-period waveforms. Geophys. J. Int. 199 (3), 1713–1738.

Moulik, P., Ekström, G., 2016. The relationships between large-scale variations in shear velocity, density, and compressional velocity in the Earth's mantle. J. Geophys. Res. 121 (4), 2737–2771.

Mound, J., Buffett, B., 2005. Mechanisms of core-mantle angular momentum exchange and the observed spectral properties of torsional oscillations. J. Geophys. Res. 110 (B8).

Mound, J. E., Buffett, B. A., 2006. Detection of a gravitational oscillation in length-of-day. Earth Planet. Sci. Lett. 243 (3-4), 383–389.

Mukhopadhyay, S., 2012. Early differentiation and volatile accretion recorded in deep-mantle neon and xenon. Nature 486 (7401), 101–104.

Mulyukova, E., Steinberger, B., Dabrowski, M., Sobolev, S. V., 2015. Survival of LLSVPs for billions of years in a vigorously convecting mantle: replenishment and destruction of chemical anomaly. J. Geophys. Res. 120 (5), 3824–3847.

Murakami, M., Hirose, K., Kawamura, K., Sata, N., Ohishi, Y., 2004. Post-perovskite phase transition in MgSiO3. Science 304 (5672), 855.

Murphy, F., Neuberg, J., Jacob, A., 1997. Alternatives to core-mantle boundary topography. Phys. Earth Planet. Inter. 103 (3-4), 349–364.

Nakagawa, T., Tackley, P. J., 2014. Influence of combined primordial layering and recycled MORB on the coupled thermal evolution of Earth's mantle and core. Geophys. Geochem. Geosys. 15 (3), 619–633.

Nakagawa, T., Tackley, P. J., Deschamps, F., Connolly, J. A., 2012. Radial 1-D seismic structures in the deep mantle in mantle convection simulations with self-consistently calculated mineralogy. Geophys. Geochem. Geosys. 13 (11).

Neuberg, J., Wahr, J., 1991. Detailed investigation of a spot on the core mantle boundary using digital PcP data. Phys. Earth Planet. Inter. 68 (1-2), 132–143.

Obayashi, M., Fukao, Y., 1997. P and PcP travel time tomography for the core-mantle boundary. J. Geophys. Res. 102 (B8), 17825.

Obayashi, M., Yoshimitsu, J., Nolet, G., Fukao, Y., Shiobara, H., Sugioka, H., Miyamachi, H., Gao, Y., 2013. Finite frequency whole mantle P wave tomography: Improvement of subducted slab images. Geophys. Res. Lett. 40 (21), 5652–5657.

Oganov, A., Ono, S., 2004. Theoretical and experimental evidence for a post-perovskite phase of MgSiO3 in Earth's D" layer. Nature 430 (6998), 445–448.

Olson, P., Deguen, R., Rudolph, M. L., Zhong, S., 2015. Core evolution driven by mantle global circulation. Phys. Earth Planet. Inter. 243, 44–55.

Panning, M., Lekić, V., Romanowicz, B., 2010. Importance of crustal corrections in the development of a new global model of radial anisotropy. J. Geophys. Res. 115 (B12).

Poupinet, G., Souriau, A., Jenatton, L., 1993. A test on the Earth's core-mantle boundary structure with antipodal data: example of Fiji-Tonga earthquakes recorded in Tamanrasset, Algeria. Geophys. J. Int. 113 (3), 684–692.

Pulliam, R. J., Stark, P. B., 1993. Bumps on the core-mantle boundary: Are they facts or artifacts? J. Geophys. Res. 98 (B2), 1943–1955.

Rekdal, T., Doornbos, D., 1992. The times and amplitudes of core phases for a variable core-mantle boundary layer. Geophys. J. Int. 108 (2), 546–556.

Resovsky, J., Ritzwoller, M., 1999. Regularization uncertainty in density models estimated from normal mode data. Geophys. Res. Lett. 26 (15), 2319–2322.

Resovsky, J. S., Ritzwoller, M. H., 1998. New and refined constraints on three-dimensional Earth structure from normal modes below 3 mHz. J. Geophys. Res. 103 (B1), 783–810.

Ritsema, J., Deuss, A., van Heijst, H.-J., Woodhouse, J. H., 2011. S40RTS: a degree-40 shear-velocity model for the mantle from new Rayleigh wave dispersion, teleseismic traveltime and normal-mode splitting function measurements. Geophys. J. Int. 184 (3), 1223–1236.

Rizo, H., Andrault, D., Bennett, N., Humayun, M., Brandon, A., Vlastélic, I., Moine, B., Poirier, A., Bouhifd, M. A., Murphy, D., 2019. 182W evidence for core-mantle interaction in the source of mantle plumes. Geochemical Perspectives Letters 11, 6–11.

Rodgers, A., Wahr, J., 1993. Inference of core-mantle boundary topography from ISC PcP and PKP traveltimes. Geophys. J. Int. 115 (3), 991–1011.

Romanowicz, B., 2001. Can we resolve 3D density heterogeneity in the lower mantle? Geophys. Res. Lett. 28 (6), 1107–1110.

Romanowicz, B., 2017. Geophysics: The buoyancy of Earth's deep mantle. Nature 551 (7680), 308.

Ros, E., Schwarz, D. J., Vocks, C., 2018. Community paper on radio astronomy infrastructures. arXiv preprint arXiv:1802.08467.

Rost, S., Revenaugh, J., 2004. Small-scale changes of core-mantle boundary reflectivity studied using core reflected PcP. Phys. Earth Planet. Inter. 145 (1-4), 19–36.

Schlaphorst, D., Thomas, C., Holme, R., Abreu, R., 2015. Investigation of core–mantle boundary topography and lowermost mantle with P4KP waves. Geophys. J. Int. 204 (2), 1060–1071.

Schubert, G., Masters, G., Olson, P., Tackley, P., 2004. Superplumes or plume clusters? Phys. Earth Planet. Inter. 146 (1-2), 147–162.

Schuberth, B., Bunge, H.-P., Steinle-Neumann, G., Moder, C., Oeser, J., 2009. Thermal versus elastic heterogeneity in high-resolution mantle circulation models with pyrolite composition: High plume excess temperatures in the lowermost mantle. Geophys. Geochem. Geosys. 10 (1).

Shearer, P. M., Hedlin, M. A., Earle, P. S., 1998. PKP and PKKP precursor observations: Implications for the small-scale structure of the deep mantle and core. In: Geophys. Monograph AGU : The Core-Mantle Boundary Region, Geodyn. Ser. Vol. 28. Wiley Online Library, pp. 37–55.

Shen, Z., Ni, S., Wu, W., Sun, D., 2016. Short period ScP phase amplitude calculations for core–mantle boundary with intermediate scale topography. Phys. Earth Planet. Inter. 253, 64–73.

Shephard, G. E., Matthews, K. J., Hosseini, K., Domeier, M., 2017. On the consistency of seismically imaged lower mantle slabs. Scientific reports 7 (1), 10976.

Simmons, N., Forte, A., Grand, S., 2009. Joint seismic, geodynamic and mineral physical constraints on three-dimensional mantle heterogeneity: Implications for the relative importance of thermal versus compositional heterogeneity. Geophys. J. Int. 177 (5), 1284–1304.

Simmons, N. A., Forte, A. M., Boschi, L., Grand, S. P., 2010. GyPSuM: A joint tomographic model of mantle density and seismic wave speeds. J. Geophys. Res. 115 (B12).

Simmons, N. A., Myers, S. C., Johannesson, G., Matzel, E., 2012. LLNL-G3Dv3: Global P wave tomography model for improved regional and teleseismic travel time prediction. J. Geophys. Res. 117 (B10).

Soldati, G., Boschi, L., 2005. The resolution of whole earth seismic tomographic models. Geophys. J. Int. 161 (1), 143–153.

Soldati, G., Boschi, L., Forte, A., 2012. Tomography of core–mantle boundary and lowermost mantle coupled by geodynamics. Geophys. J. Int. 189 (2), 730–746.

Soldati, G., Boschi, L., Piersanti, A., 2003. Outer core density heterogeneity and the discrepancy between PKP and PcP travel time observations. Geophys. Res. Lett. 30 (4), 1190.

Soldati, G., Koelemeijer, P., Boschi, L., Deuss, A., 2013. Constraints on core-mantle boundary topography from normal mode splitting. Geophys. Geochem. Geosys. 14 (5), 1333–1342.

Stark, P. B., Hengartner, N. W., 1993. Reproducing Earth's kernel: Uncertainty of the shape of the core-mantle boundary from PKP and PcP travel times. J. Geophys. Res. 98 (B2), 1957–1971.

Steinberger, B., Holme, R., 2008. Mantle flow models with core-mantle boundary constraints and chemical heterogeneities in the lowermost mantle. J. Geophys. Res. 113 (B5).

Styles, E., Davies, D. R., Goes, S., 2011. Mapping spherical seismic into physical structure: biases from 3D phase-transition and thermal boundary-layer heterogeneity. Geophys. J. Int. 184 (3), 1371–1378.

Su, W., Dziewonski, A., 1997. Simultaneous inversion for 3-D variations in shear and bulk velocity in the mantle. Phys. Earth Planet. Inter. 100 (1-4), 135–156.

Sze, E., van der Hilst, R., 2003. Core mantle boundary topography from short period PcP, PKP, and PKKP data. Phys. Earth Planet. Inter. 135 (1), 27–46.

Tackley, P. J., 2002. Strong heterogeneity caused by deep mantle layering. Geophys. Geochem. Geosys. 3 (4), 1–22.

Tan, E., Gurnis, M., 2005. Metastable superplumes and mantle compressibility. Geophys. Res. Lett. 32 (20).

Tanaka, S., 2010. Constraints on the core-mantle boundary topography from P4KP-PcP differential travel times. J. Geophys. Res. 115 (B4), B04310.

Tarduno, J. A., Watkeys, M. K., Huffman, T. N., Cottrell, R. D., Blackman, E. G., Wendt, A., Scribner, C. A., Wagner, C. L., 2015. Antiquity of the South Atlantic Anomaly and evidence for top-down control on the geodynamo. Nature Comm. 6, 7865.

Tesoniero, A., Auer, L., Boschi, L., Cammarano, F., 2015. Hydration of marginal basins and compositional variations within the continental lithospheric mantle inferred from a new global model of shear and compressional velocity. J. Geophys. Res. 120 (11), 7789–7813.

Tesoniero, A., Cammarano, F., Boschi, L., 2016. S- to- P heterogeneity ratio in the lower mantle and thermo-chemical implications. Geophys. Geochem. Geosys. 17 (7), 2522–2538.

Torsvik, T. H., Burke, K., Steinberger, B., Webb, S. J., Ashwal, L. D., 2010. Diamonds sampled by plumes from the core-mantle boundary. Nature 466 (7304), 352–355.

Trampert, J., Deschamps, F., Resovsky, J., Yuen, D., 2004. Probabilistic tomography maps chemical heterogeneities throughout the lower mantle. Science 306 (5697), 853.

Tromp, J., Zanzerkia, E., 1995. Toroidal splitting observations from the great 1994 Bolivia and Kuril Islands earthquakes. Geophys. Res. Lett. 22 (16), 2297–2300.

Tsuchiya, T., Tsuchiya, J., Umemoto, K., Wentzcovitch, R., 2004. Phase transition in MgSiO3 perovskite in the Earth's lower mantle. Earth Planet. Sci. Lett. 224 (3-4), 241–248.

Van den Berg, A., Cloetingh, S., Doornbos, D., 1978. A comparison of PKP precursor data from several seismic arrays. J. Geophys. Res. 44, 499–510.

Vasco, D., Johnson, L. R., Marques, O., 1999. Global Earth structure: inference and assessment. Geophys. J. Int. 137 (2), 381–407.

Ventosa, S., Romanowicz, B., 2015. Extraction of weak PcP phases using the slant-stacklet transform–II: constraints on lateral variations of structure near the core–mantle boundary. Geophys. J. Int. 203 (2), 1227–1245.

Vidale, J. E., Benz, H. M., 1992. A sharp and flat section of the core–mantle boundary. Nature 359 (6396), 627.

Wahr, J., De Vries, D., 1989. The possibility of lateral structure inside the core and its implications for nutation and Earth tide observations. Geophys. J. Int. 99 (3), 511–519.

Wessel, P., Smith, W. H. F., Scharroo, R., Luis, J., Wobbe, F., 2013. Generic mapping tools: Improved version released. Eos, Transactions American Geophysical Union 94 (45), 409–410.

Wu, W., Ni, S., Shen, Z., 2014. Constraining the short scale core–mantle boundary topography beneath Kenai Peninsula (Alaska) with amplitudes of core-reflected PcP wave. Phys. Earth Planet. Inter. 236, 60–68.

Yoshida, M., 2008. Core-mantle boundary topography estimated from numerical simulations of instantaneous mantle flow. Geophys. Geochem. Geosys. 9 (7).

Zhang, N., Zhong, S., 2011. Heat fluxes at the Earth's surface and core–mantle boundary since Pangea formation and their implications for the geomagnetic superchrons. Earth Planet. Sci. Lett. 306 (3-4), 205–216.

Zindler, A., Hart, S., 1986. Chemical geodynamics. Ann. Rev. Earth Planet Sci. 14, 493–571.

Tables

Constraints on CMB topography amplitude **Reference**	**Data / methodology**	**Region**	**Length scale**	**Amplitude**
Haddon and Cleary (1974)	PKP precursors	Regional	30 km	Few 100 m
Aleshin and Vinnik (1975)	PKP precursors, PmKP reflections	Regional	10 km	10 km
Doornbos (1978)	PKP precursors	Regional	10–20 km	200 m
Chang and Cleary (1978)	PKKP precursors	Regional		Few km
Doornbos (1980)	PKKP precursors	Regional	10-20 km	100–200 m
Chang and Cleary (1981)	PKKP precursors	Regional		Few km
Menke (1986)	PcP amplitudes	Regional	10 km	Few 100 m
Bataille and Flatté (1988)	PKP precursors	Regional		300 m
Gudmundsson (1989)	PcP, $PKP_{ab,bc,cd,df}$	Regional		4 km PTP
Bataille et al. (1990)	PKP, PKKP, PKIKP precursors	Global patches		300 m
Neuberg and Wahr (1991)	PcP - P, PcP / P amplitude ratio	Regional	50–400 km	2–3 km
Vidale and Benz (1992)	PcP, ScP	Regional	50–200 km	<500 m
Poupinet et al. (1993)	PKP_{ab}-PKIKP	Regional		<4 km
Earle and Shearer (1998)	PKKP precursors	Regional	7–10 km	0.35 km
Shearer et al. (1998)	PKKP precursors	Regional	8 (20) km	300 (600) m
Garcia and Souriau (2000)	PcP, PKP_{bc}, $PKKP_{bc}$	Global patches	300–1500 km	95 % below 4 km
Koper et al. (2003)	PKiKP - PcP	Regional		3.5 km PTP
Colombi et al. (2014)	PcP, ScS, P_{diff}, PKP_{df}, SKS_{ac}	Global	Y_{lm}, $l \leq 10$	7 km PTP
Wu et al. (2014)	PcP	Regional	300–400 km	6 km
Ventosa and Romanowicz (2015)	PcP - P	Regional		2.7 km
Schlaphorst et al. (2015)	P4KP - PKP	Regional	150 km	60 km over 3 points
Mancinelli and Shearer (2016)	PKKP precursors	Regional	7 km	390 m
Shen et al. (2016)	PcP, ScP	Regional	140 km	1.2 km
Hide and Horai (1968)	Geoid modelling	Global	Y_{lm}, $l \leq 4$	8.7 km PTP
Hager et al. (1985)	Geoid modelling	Global	Y_{lm}, $l = 2, 3$	<3 km
Gwinn et al. (1986)	Nutation measurements (VLBI)	Global	Y_{20} only	490 m
Wahr and De Vries (1989)	Nutation measurements (VLBI)	Global	Y_{20} only	0.5-0.87 km
Jault and Le Mouël (1990)	Dynamic flow modelling	Global	Odd Y_{lm}, $l \leq 5$	11.9 km PTP
Forte and Peltier (1991)	Seismic-geodynamic modelling	Global	Y_{lm}, $l \leq 4$	<8 km
Forte et al. (1995)	Seismic-geodynamic modelling	Global	Y_{lm}, $l \leq 8$	<6 km
Mathews et al. (2002)	Nutation measurements (VLBI)	Global	Y_{20} only	390 m
Forte (2007)	Seismic-geodynamic modelling	Global	Y_{lm}, $l \leq 20$	2.6 km PTP
Steinberger and Holme (2008)	Seismic-geodynamic modelling	Global	Y_{lm}, $l \leq 15$	6 km PTP

Simmons et al. (2009)		Joint seismic-geodynamic-mineralogical inversion	Global	275 km blocks	3.5 km PTP
Koelemeijer et al. (2012)		Lower mantle sensitive modes c_{st}	Global	Y_{lm}, $l = 2$ only	5 km PTP

Global CMB topography models

Reference	Model name	Data	Velocity model	Parameterisation	PTP amplitude
Creager and Jordan (1986)	CJ1986	$PKP_{ab,df}$	M84C + thin layers	All Y_{lm}, $l \leq 5$	20.1 km
Morelli and Dziewonski (1987)	***MD1987***	PcP,PKP_{bc}	HELM46	All Y_{lm}, $l \leq 4$	12.3 km
Doornbos and Hilton (1989)	***DH1989-M6***	PcP, $PKP_{ab,bc}$, $PKKP_{bc}$, $PnKP_{ab}$	M84C + thin layer	All Y_{lm}, $l \leq 4$	7.7 km
Doornbos and Hilton (1989)	DH1989-M7	PcP, $PKP_{ab,bc}$, $PKKP_{bc}$, $PnKP_{ab}$	M84C	All Y_{lm}, $l \leq 4$	8.3 km
Obayashi and Fukao (1997)	OF1997	P, PcP	Own V_P	All Y_{lm}, $l \leq 5$	14 km / 4 km
Vasco et al. (1999)	Vetal1999	P, S, PP, PcP, SS, ScS, $PKP_{ab,bc,df}$ SKS_{ac}, SS-S410S, SS-S660S	Own V_S, V_P	2° equal area	12 km
Boschi and Dziewonski (2000)	BD2000	P, PcP, $PKP_{bc,df}$	Own V_P	5° equal area	<20 km
Soldati et al. (2003)	Setal2003	P, PcP, $PKP_{bc,df}$	Own V_P	1656 equal area blocks	<20 km
Sze and van der Hilst (2003)	***SV2003***	PcP, $PKP_{ab,bc,df}$, $PKKP_{ab,bc}$	KH2001	All Y_{lm}, $l \leq 4$	2.4 km
Tanaka (2010)	***T2010***	P4KP - PcP	PMEAN + layer	Even Y_{lm}, $l \leq 4$	4.5 km
Soldati et al. (2012)	***SBF2012-T***	P, PcP, $PKP_{bc,df}$	Own V_P	5° equal area	12.4 km
Soldati et al. (2012)	Setal2012-TG	P, PcP, $PKP_{bc,df}$ with geodynamic coupling	Own V_P	5° equal area	8.7 km
Soldati et al. (2012)	***SBF2012-TGppv***	P, PcP, $PKP_{bc,df}$ with geodynamic coupling	Own V_P	5° equal area	2.1 km
Li et al. (1991)	***LGW1991-SAT***	Normal modes spectra	Own V_S	Even Y_{lm}, $l \leq 4$	3.7 km
Li et al. (1991)	***LGW1991-SAF***	Normal modes c_{st}	Own V_S	Even Y_{lm}, $l \leq 4$	5.2 km
Ishii and Tromp (1999)	***IT1999***	Normal modes c_{st}, gravity	Own V_S, V_P	Even Y_{lm}, $l \leq 6$	14.4 km
Koelemeijer et al. (2017)	KDR2017-neg	Stoneley modes c_{st}	SP12RTS	Even Y_{lm}, $l \leq 6$	4.7 km
Koelemeijer et al. (2017)	KDR2017-pos	Stoneley modes c_{st}	SP12RTS	Even Y_{lm}, $l \leq 6$	5.7 km
Koelemeijer et al. (2017)	***KDR2017***	Stoneley modes c_{st}	SP12RTS	Even Y_{lm}, $l \leq 6$	5.7 km

Global density models

Reference	Model name	Data	Velocity model	Lateral param.	Vertical param.
Ishii and Tromp (1999)	***IT1999***	Normal modes c_{st}, gravity	Own V_S, V_P	Even Y_{lm}, $l \leq 6$	Chebychev polynomials to order 13
Trampert et al. (2004)	***Tetal2004***	Surface waves, normal modes c_{st}, gravity	Own V_S, V_P	Even Y_{lm}, $l \leq 6$	5 constant layers
Mosca et al. (2012)	***Metal2012***	Surface waves, body waves, normal modes c_{st}	Own V_S, V_P	Even Y_{lm}, $l \leq 6$	10 cubic splines

Moulik and Ekström (2016)	***ME2016***	Surface waves, body waves, normal modes c_{st}, waveforms	Own V_S, V_P	362 spherical splines	16 cubic splines
Lau et al. (2017)	***Letal2017***	Tidal GPS measurements	S40RTS	2 scaling factors	3 constant layers
Koelemeijer et al. (2017)	***KDR2017-neg***	Stoneley modes c_{st}	SP12RTS	2 scaling factors	1-2 constant layers
Koelemeijer et al. (2017)	***KDR2017-pos***	Stoneley modes c_{st}	SP12RTS	2 scaling factors	1-2 constant layers
Koelemeijer et al. (2017)	KDR2017-all	Stoneley modes c_{st}	SP12RTS	2 scaling factors	1-2 constant layers

Table 1: Overview of past observational studies of CMB topography and density. Note that for global CMB topography models, the peak-to-peak (PTP) amplitude is indicated, while for other constraints the amplitude is given instead (unless otherwise specified). The length scale generally relates to the period of the waves used in the study, and indicates either the wavelength or the correlation length. c_{st} stands for splitting function measurements, while Y_{lm} indicates spherical harmonics up to maximum degree l. Models in bold italic are used in the current study in the computation of average models and vote maps.

Figures

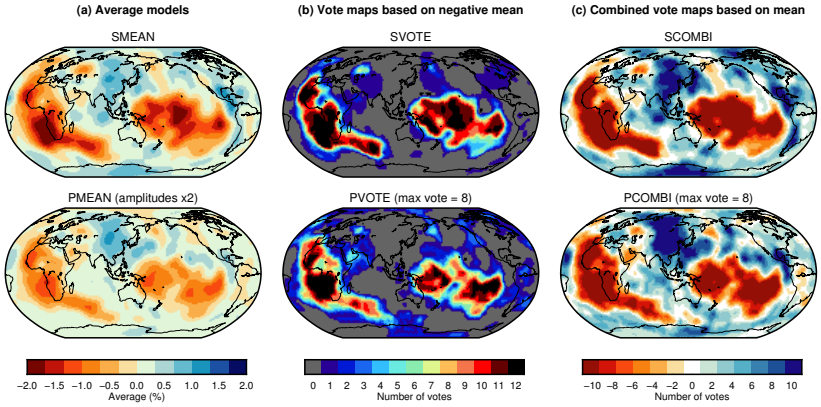

Figure 1: Typical long-wavelength (up to spherical harmonic degree 12) velocity structure at 2800 km depth showing (top) V_S and (bottom) V_P showing (a) average models ("MEAN") similarly to Becker and Boschi (2002), (b) vote maps ("VOTE") based on negative velocity anomalies and (c) combined vote maps based on both positive and negative velocity anomalies ("COMBI"), computed following Shephard et al. (2017). Only models developed since 2010 have been included, resulting in 12 models for V_S: GYPSUM-S (Simmons et al., 2010), SAW642ANb (Panning et al., 2010), S40RTS (Ritsema et al., 2011), METAL12-S (Mosca et al., 2012), S362ANI+M (Moulik and Ekström, 2014), SAVANI (Auer et al., 2014), SEMUCB-WM1 (French and Romanowicz, 2014), SGLOBE-rani (Chang et al., 2015), SPani-S (Tesoniero et al., 2015), SP12RTS-S (Koelemeijer et al., 2016), TX2015 (Lu and Grand, 2016) and SEISGLOBE2 (Durand et al., 2017). 8 V_P models are included: GYPSUM-P (Simmons et al., 2010), LLNL_G3Dv3 (Simmons et al., 2012), METAL12-P (Mosca et al., 2012), GAP-P4 (Obayashi et al., 2013), SPani-P (Tesoniero et al., 2015), SP12RTS-P (Koelemeijer et al., 2016), MIT2016 (Burdick et al., 2017) and H2016 (Hosseini, 2016). It is evident that the LLVPs are imaged consistently across both S- and P-wave models.

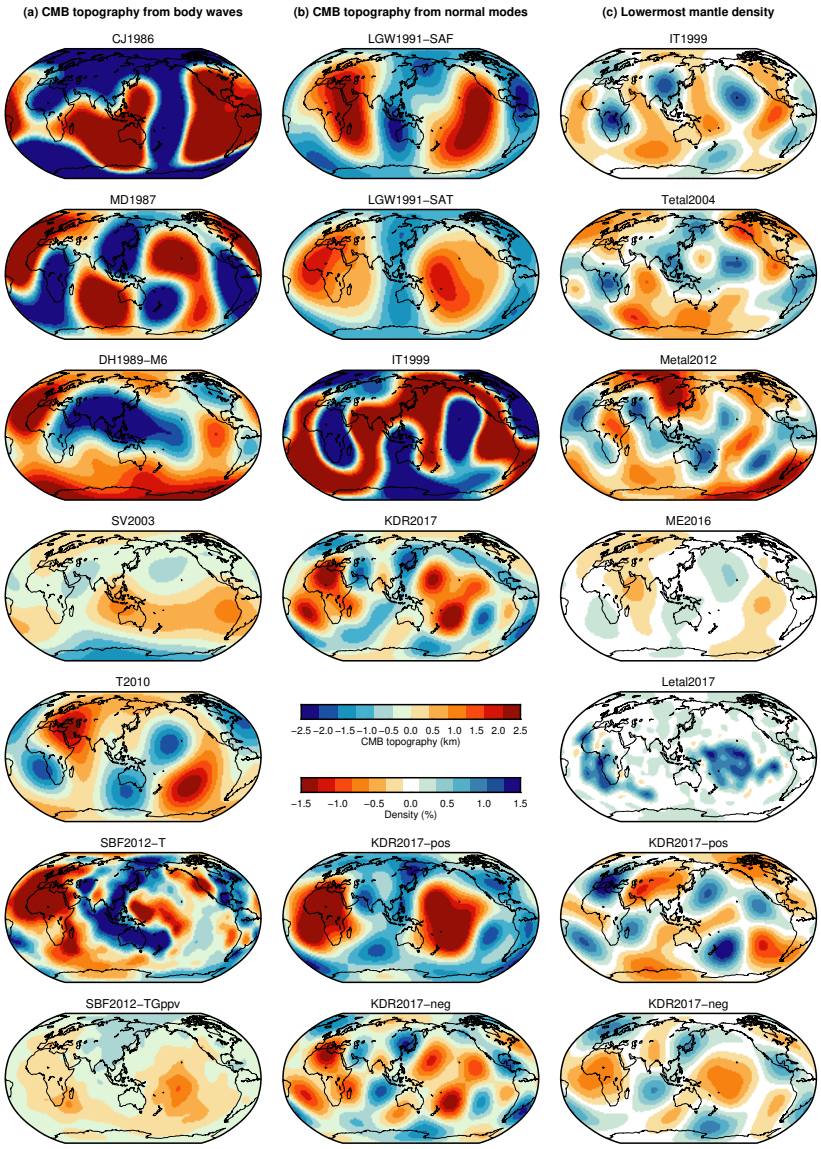

Figure 2: Overview of global (a–b) CMB topography models and (c) lowermost mantle density structure at 2800 km depth. CMB topography models are derived from (a) body-wave data (CJ1986 (Creager and Jordan, 1986), MD1987 (Morelli and Dziewonski, 1987), DH1989-M6 (Doornbos and Hilton, 1989), SV2003 (Sze and van der Hilst, 2003), T2010 (Tanaka, 2010), SBF2012-T and SBF2012-TGppv (Soldati et al., 2012)) or (b) normal-mode data (LGW1991-SAF and LGW1991-SAT (Li et al., 1991), IT1999 (Ishii and Tromp, 1999) and KDR2017, KDR2017-pos and KDR2017-neg (Koelemeijer et al., 2017) - with the latter two only included for comparison to the density models). Density models are primarily constrained by normal-mode data combined with other seismic data (IT1999 (Ishii and Tromp, 1999), Tetal2004 (the mean model of Trampert et al., 2004), Metal2012 (the mean model of Mosca et al., 2012), ME2016 (Moulik and Ekström, 2016), KDR2017-pos and KDR2017-neg (the best fitting models of Koelemeijer et al., 2017)) or derived from Earth's tides (Letal2017, the mean model of Lau et al. (2017)). CMB topography models based on body-wave data (a) show a large variety in both pattern and amplitude, while those derived from normal modes (b) generally show elevated topography for the LLVP locations (with IT1999 the odd one out). Density models (c) differ in detail, but most models have dense LLVPs (with the exception of KDR2017-neg). Note that the maximum degree of the spherical harmonic expansion differs between models (as detailed in Table 1.

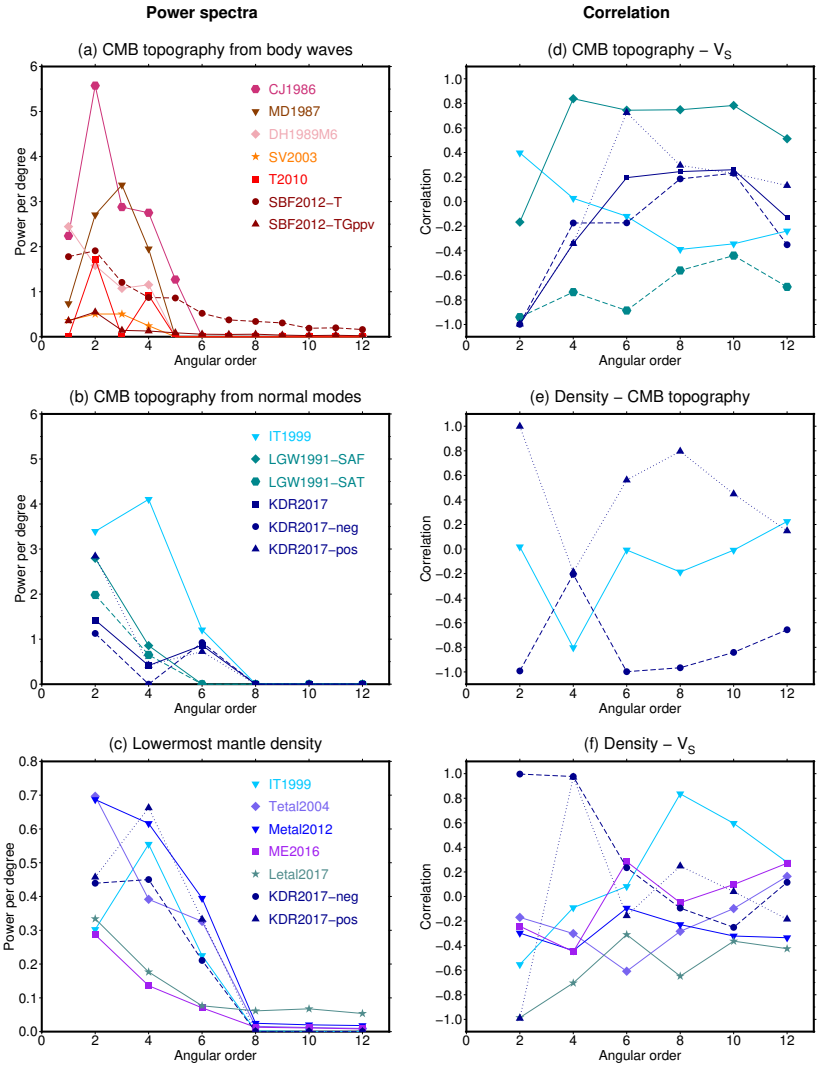

Figure 3: Properties of global CMB topography and density models shown in Figure 2 and listed in Table 1, showing (a–c) the power spectra of individual models and (d–f) the correlation between different model properties: (d) V_S structure and CMB topography, (e) density and CMB topography and (f) density and V_S structure. The correlation is only computed when both properties are provided in a consistent manner. Topography models KDR2017-neg and KDR2017-pos are best-fitting models, only shown to demonstrate their relationship to the corresponding density models, while mean models are used for Tetal2004, Metal2012 and Letal2017. For CMB topography models based on body waves (a), models with large amplitudes are typically older (developed prior to 2000), while newer models show smaller amplitudes. The IT2001 model shows a larger power in degree 4 (b) than most other models. Amplitudes of density models (c) vary with smaller power in degree 4 (Moulik and Ekström, 2016; Lau et al., 2017) or larger degree 4 power (all other models). The correlation between CMB topography models and V_S structure (d) in the lowermost mantle tends to be negative for degree 2 except for the IT1999 model. Only few models exist that provide both CMB topography and density structure (e) in a consistent way, with the models by Koelemeijer et al. (2017) showing a clear opposite relationship for degree 2. Most density models have the same relationship with V_S (f), except the KDR2017-neg model. Note that KDR2017-pos and Letal2017 have a similar degree 2 correlation between density and V_S.

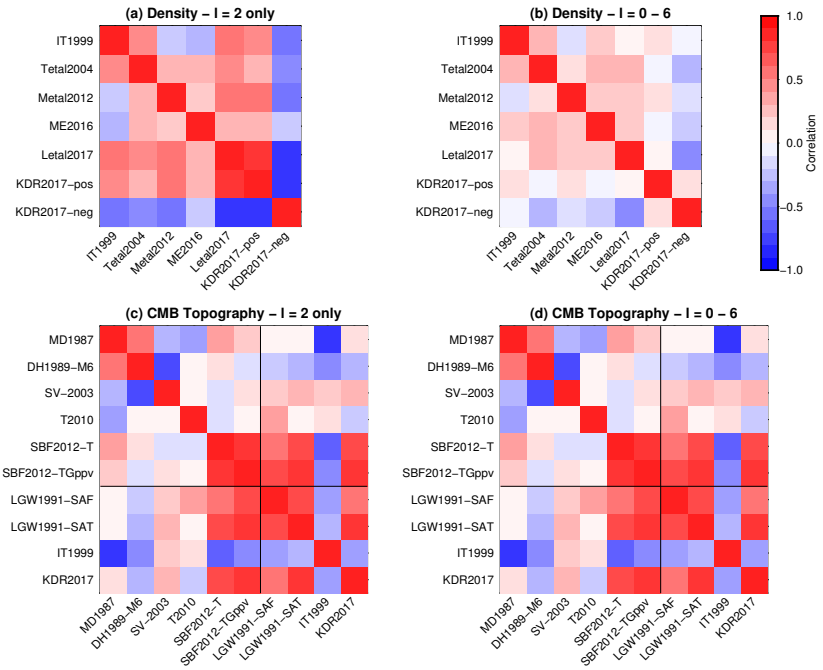

Figure 4: Cross-model correlation for global models included in Table 1 of (a–b) lowermost mantle density structure and (c–d) CMB topography, showing (a,c) the correlation for degree 2 structure only and (b,d) the correlation for structure up to degree 6. The thin black lines in (c–d) separate out body-wave models (top left) and normal-mode models (bottom right). Density models show a high cross-model correlation (particularly between Letal2017 and KDR2017-pos), with the exception of KDR2017-neg. Body-wave models of CMB topography do not show much consistency, but normal-mode models (except IT1999) have a high correlation. For structure up to degree 6, results are similar for CMB topography, whereas the correlation values are lower (albeit still positive) for density.

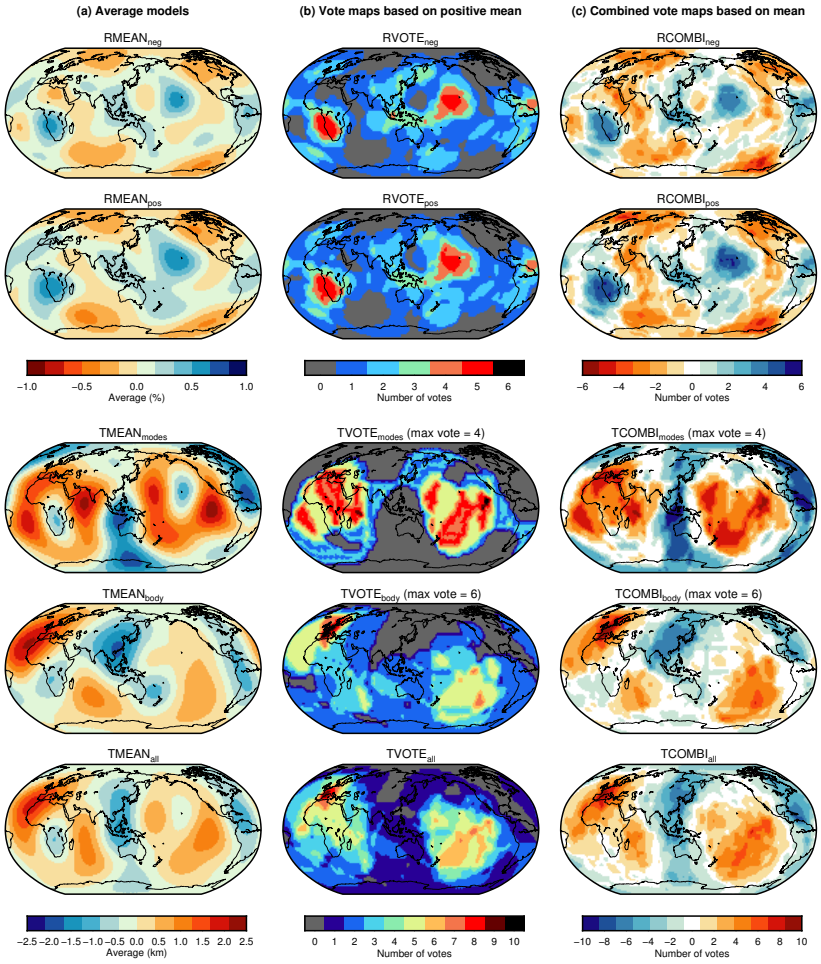

Figure 5: Summary models of lowermost mantle density structure (top two rows) and CMB topography (bottom three rows) based on global models indicated in bold in Table 1, showing (a) average models ("MEAN") computed similarly to Becker and Boschi (2002), (b) vote maps based on positive anomalies ("VOTE") and (c) combined vote maps based on both positive and negative anomalies ("COMBI"), computed following Shephard et al. (2017). For density, the only difference between the top and bottom row is the inclusion of KDR2017-neg instead of KDR2017-pos besides 5 other models. For CMB topography, summary models are shown for models based on normal-mode data (including the KDR2017 model), based on body-wave data or using all models. In the computation of average models, amplitudes are included and it is possible for one model to dominate the results, while vote maps are only based on patterns and amplitude distribution within the models. Note the difference in maximum vote for vote maps based on body-wave (6) and normal-mode (4) data.

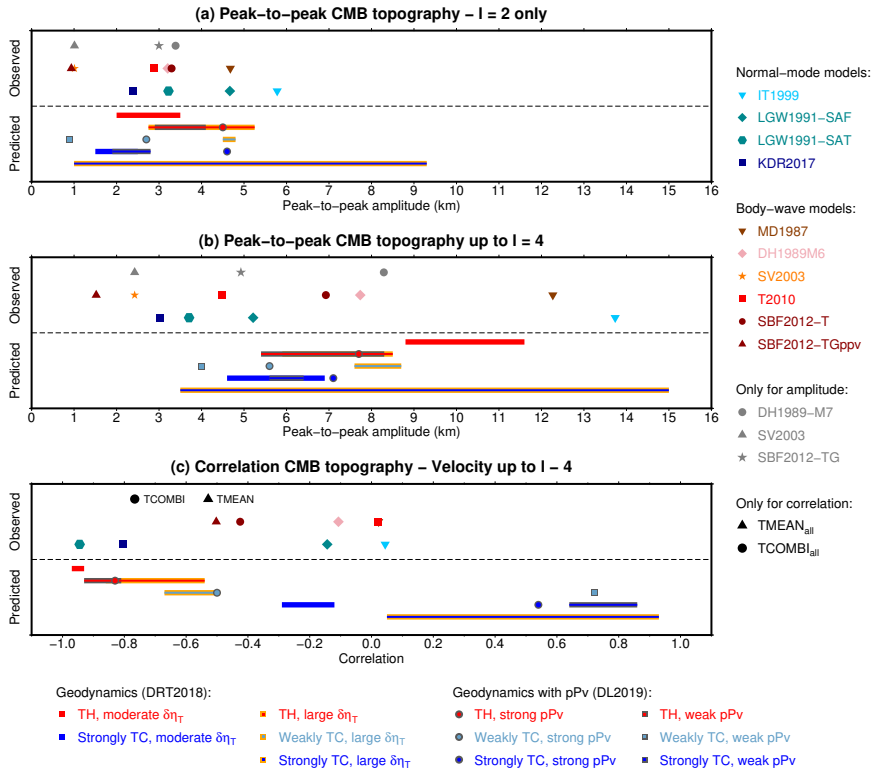

Figure 6: Comparison between seismic constraints and geodynamic predictions calculated on the same length scales, showing (a) degree 2 and (b) degree 4 peak-to-peak CMB topography amplitudes and (c) the correlation of topography with velocity structure at 2800 km depth. Geodynamic predictions are taken from Deschamps et al. (2018, DRT2018) and Deschamps and Li (2019, DL2019). DRT2018 computed properties for purely thermal (TH) models and strongly thermochemical (TC) models ($\delta\rho_C \geq 100$ kg/m^3) with a moderate ($\delta\eta_T = 10^6$) or large ($\delta\eta_T \geq 10^9$) thermal viscosity contrast, as well as for a weak TC model ($\delta\rho_C \leq 100$ kg/m^3) with a strong thermal viscosity contrast ($\delta\eta_T \geq 10^9$). DL2019 followed up on these results by including post-perovskite (pPv) with a viscosity difference of 1 (strong pPv) or ranging between 10^{-1} and 10^{-3} (weak pPv) at the same time as a large thermal viscosity contrast ($\delta\eta_T \geq 10^9$). The correlation between velocity and CMB topographic variations is only computed for models that provide both or use a known velocity model. I compute the correlation with V_S variations for normal-mode models, whereas for body-wave models I show the correlation with V_P variations, as these are constructed from P-wave sensitive data. Given the large positive correlation between lower mantle P- and S-wave models, this does not make a large difference. Corresponding values for the average models and vote map developed in this study (TMEAN–SMEAN and TCOMBI–SCOMBI) are shown as well. These are only given for topography-velocity correlation (c), as amplitudes are only constrained in average models, which are biased by particular large-amplitude models.